Journal of Computational Physics 445 (2021) 110596

Contents lists available at ScienceDirect

Journal of Computational Physics

www.elsevier.com/locate/jcp

Positivity-preserving high order finite volume hybrid Hermite WENO schemes for compressible Navier-Stokes equations ☆

Chuan Fan [a], Xiangxiong Zhang [b], Jianxian Qiu [c,*]

[a] School of Mathematical Sciences, Xiamen University, Xiamen, Fujian 361005, PR China
[b] Department of Mathematics, Purdue University, West Lafayette, IN 47907-2067, USA
[c] School of Mathematical Sciences and Fujian Provincial Key Laboratory of Mathematical Modeling and High-Performance Scientific Computing, Xiamen University, Xiamen, Fujian 361005, PR China

ARTICLE INFO

Article history:
Available online 30 July 2021

Keywords:
Positivity-preserving
Hybrid HWENO schemes
Finite volume scheme
Compressible Navier-Stokes equations

ABSTRACT

In this paper, we construct a positivity-preserving high order accurate finite volume hybrid Hermite Weighted Essentially Non-oscillatory (HWENO) scheme for compressible Navier-Stokes equations, by incorporating a nonlinear flux and a positivity-preserving limiter. HWENO schemes have more compact stencils than WENO schemes but with higher computational cost due to the auxiliary variables. The hybrid HWENO schemes use linear reconstructions in smooth region thus are more efficient than conventional HWENO schemes. However, the hybrid HWENO is not robust for many demanding problems. The positivity-preserving hybrid HWENO scheme in this paper is not only more efficient but also much more robust than the conventional HWENO method for both compressible Euler and compressible Navier-Stokes equations, especially for solving gas dynamics equations in low density and low pressure regime. Numerical tests on low density and low pressure problems are performed to demonstrate the robustness and the efficiency of the positivity-preserving hybrid HWENO scheme.

1. Introduction

The compressible Euler equations and Navier-Stokes equations are the most popular continuum equations in the modeling and analysis of gas dynamics problems. The positivity of density and pressure are crucial to robustness of numerical simulations, in many applications such as aerospace, meteorology, oceanography, hydraulic engineering, chemical engineering, etc. It is often necessary to preserve the positivity of density and pressure for constructing robust high order numerical schemes solving demanding gas dynamics problems, especially for problems involving both shocks and low density and low pressure.

In the past decade, quite a few successful positivity-preserving high-order schemes for solving compressible Euler equations have been constructed, including positivity-preserving discontinuous Galerkin (DG) scheme proposed by Zhang and Shu in [28,29], the positivity-preserving finite difference Weighted Essential Non-oscillatory (WENO) schemes in [8,25,30], as well as positivity-preserving finite volume WENO schemes in [7,8]. On the other hand, the positivity-preserving property in these high order methods for compressible Euler equations does not hold for the additional diffusion term in the

☆ C. Fan and J. Qiu were supported by NSFC grant 12071392. X. Zhang was supported by the NSF grant DMS-1913120.
* Corresponding author.
E-mail addresses: fanchuan@stu.xmu.edu.cn (C. Fan), zhan1966@purdue.edu (X. Zhang), jxqiu@xmu.edu.cn (J. Qiu).

https://doi.org/10.1016/j.jcp.2021.110596
0021-9991/

compressible Navier-Stokes equations. Even though many popular high order accurate schemes can be rendered positivity-preserving for a pure convection problem such as compressible Euler equations, it is challenging to extend these methods to a convection diffusion problem. For popular linear schemes including conventional finite volume methods and most DG schemes for solving scalar diffusion equations, positivity-preserving or bound-preserving can be enforced in the same fashion as in positivity-preserving high order schemes for compressible Euler equations, up to at most second order accuracy [26,31]. Though there are a few bound-preserving linear higher order accurate schemes for scalar diffusion equations [4,5,10,27], it is quite difficult to extend these methods to the complicated compressible Navier-Stokes system. In general, for solving compressible Navier-Stokes equations, it is nontrivial to adopt the bound-preserving discretization of scalar diffusion operators or positivity-preserving techniques for compressible Euler system. In [26], Zhang first constructed a uniformly high order accurate positivity-preserving DG scheme for solving compressible Navier-Stokes equations, which can be easily and efficiently implemented in multiple dimensions. The key ingredients include a nonlinear diffusion flux and a positivity-preserving limiter, which also applies to finite volume schemes.

The finite volume (FV) Hermite WENO (HWENO) schemes were first proposed by Qiu and Shu in [18] and initially used as a limiter for stabilizing Runge-Kutta DG methods. Since then, many HWENO schemes have been developed to solve hyperbolic conservation laws and related problems, including FV HWENO schemes in [2,3,22,23,37] and FD HWENO schemes in [11,12] for hyperbolic conservation law, as a limiter for DG methods in [15–17,19,38,42], applications for the Hamilton-Jacobi equation in [20,24,34–36,39–41], Vlasov equations in [1], KdV equation in [14], etc. Compared to WENO schemes, the major advantages of HWENO schemes include more compact stencil thus easier treatment of the boundary conditions, and higher resolution in numerical solutions for schemes of the same order. However, in practice HWENO schemes are less robust than WENO schemes, with higher computational cost due to the additional derivative equation. To improve robustness and computational efficiency, Zhao and Qiu proposed a high order FV hybrid HWENO schemes in [32,33], in which the Hermite type reconstruction is based on zeroth-order moment, i.e., the cell averages, and first-order moment reconstruction. Here *hybrid* refers to the hybridization of nonlinear and linear reconstructions, i.e., the nonlinear HWENO reconstruction is only used on troubled cells defined by some discontinuity detector and linear reconstruction is used on the other cells. Such hybrid schemes can save computational cost since linear reconstructions are more efficient than nonlinear ones. In [32,33], an additional limiter suppressing oscillations is applied on the first-order moment, coupled with the HWENO reconstruction, thus such a hybrid HWENO scheme is also more robust than the original HWENO scheme, but it is still unstable for many low density and low pressure problems.

In this paper, we design a positivity-preserving high order FV hybrid HWENO scheme, based on the work in [26,32], to solve compressible Navier-Stokes equations. When the Reynolds number is infinity and the viscous term disappears, it also reduces a positivity-preserving high order scheme for compressible Euler equations. The positivity-preserving finite volume HWENO scheme for solving compressible Euler equations in [2] was based on the reconstruction of the function cell averages and derivative cell averages, where two sets of stencil are used to approximate the function point values and derivative point values for spatial reconstruction. The positivity-preserving high order FV hybrid HWENO scheme in this paper is based on zeroth-order moment and first-order moment reconstruction, with only one set of stencil for spatial reconstruction. Compared with the reconstruction in [2], the hybrid HWENO scheme in this paper has less computational cost due to the hybridization techniques using only linear reconstruction for smooth regions.

The rest of the paper is organized as follows. In Section 2, we briefly describe the hybrid HWENO schemes for solving compressible Navier-Stokes equations. In Section 3, we introduce the positivity-preserving finite volume hybrid HWENO scheme for one-dimensional and two-dimensional compressible Navier-Stokes equations. Numerical tests are given in Section 4. Concluding remarks are given by Section 5.

2. Finite volume hybrid Hermite WENO schemes

The dimensionless compressible Navier-Stokes equations for ideal gases in [26] in conservative form can be written as

$$\mathbf{U}_t + \nabla \cdot \mathbf{F}(\mathbf{U}, \mathbf{S}) = 0, \tag{2.1}$$

where $\mathbf{U} = (\rho, \rho\mathbf{u}, E)^T$ are conservative variables with the velocity $\mathbf{u} = (u, v, w)$, ρ is the density, E is the total energy and the superscript T denotes transpose of a vector. Let $\mathbf{S} = \nabla\mathbf{U}$ denote the derivative. The flux function $\mathbf{F}(\mathbf{U}, \mathbf{S}) = \mathbf{F}^a - \mathbf{F}^d$ consists of the advection and the diffusion fluxes:

$$\mathbf{F}^a = \begin{pmatrix} \rho\mathbf{u} \\ \rho\mathbf{u}\otimes\mathbf{u} + p\mathbb{I} \\ (E+p)\mathbf{u} \end{pmatrix}, \mathbf{F}^d = \begin{pmatrix} 0 \\ \boldsymbol{\tau} \\ \mathbf{u}\cdot\boldsymbol{\tau} - \mathbf{q} \end{pmatrix}, \tag{2.2}$$

where p is pressure, $\mathbb{I}$ is the unit tensor, the dimensionless stress tensor is given by $\boldsymbol{\tau} = \frac{1}{\mathrm{Re}}\left(\nabla\mathbf{u} + (\nabla\mathbf{u})^T - \frac{2}{3}(\nabla\cdot\mathbf{u})\mathbb{I}\right)$ with the Reynolds number Re, and $\mathbf{q} = -\kappa\nabla T$ denotes the heat diffusion flux with the thermal conductivity coefficient κ proportional to $\frac{1}{\mathrm{Re}}$ in molecular theory. Assuming the specific heat at constant pressure c_p is a constant, the dimensionless quantity Prandtl number $\mathrm{Pr} = \frac{c_p}{\kappa\mathrm{Re}}$ is a constant. For the ideal gas, the total energy $E = \frac{1}{2}\rho||\mathbf{u}||^2 + \rho e$ where e denotes

the internal energy, $p=(\gamma-1)\rho e$ and $T=\frac{e}{c_v}$ where the specific heat capacity c_v and ratio of specific heats $\gamma=\frac{c_p}{c_v}$ are constants. We will use $\gamma=1.4$ and $\mathrm{Pr}=0.72$ for air.

After multiplying (2.1) by the test function $\phi(x)$ and integration by part on a rectangular cell K, we can obtain the following integral form

$$\frac{\mathrm{d}}{\mathrm{d}t}\int_K \mathbf{U}(x,t)\phi(x)dx=-\int_{\partial K}(\mathbf{F}\cdot\mathbf{n})\phi(x)ds+\int_K(\mathbf{F}\cdot\nabla\phi)dx, \tag{2.3}$$

where $\mathbf{n}$ represents the outward unit vector normal to the boundary of the cell ∂K. In the one dimensional case, the cell K is an interval $[x_{i-\frac{1}{2}},x_{i+\frac{1}{2}}]$ and the test function $\phi(x)$ is taken as $\frac{1}{\Delta x}$ and $\frac{x-x_j}{(\Delta x)^2}$. In the two dimensional case, the cell K is a rectangle $[x_{i-\frac{1}{2}},x_{i+\frac{1}{2}}]\times[y_{j-\frac{1}{2}},y_{j+\frac{1}{2}}]$ and the test function $\phi(x)$ is taken as $\frac{1}{\Delta x\Delta y}$, $\frac{x-x_i}{(\Delta x)^2\Delta y}$ and $\frac{y-y_j}{\Delta x(\Delta y)^2}$. The line integral in (2.3) can be approximated by a L-points Gauss quadrature on each edge of $\partial K=\bigcup_{s=1}^{S}\partial K_s$

$$\int_{\partial K}(\mathbf{F}\cdot\mathbf{n})\phi(x)ds\approx\sum_{s=1}^{S}|\partial K_s|\sum_{\ell=1}^{L}\omega_\ell[\mathbf{F}(\mathbf{U}(G_{s\ell},t),\mathbf{S}(\mathbf{U}_{s\ell},t))\cdot\mathbf{n}]\phi(G_{s\ell}) \tag{2.4}$$

where $G_{s\ell}$ and ω_ℓ are Gauss quadrature points on the edge ∂K_{is} and normalized weights respectively. The flux $\mathbf{F}(\mathbf{U}(G_{s\ell},t),\mathbf{S}(\mathbf{U}_{s\ell},t))\cdot\mathbf{n}$ at Gauss quadrature points should be replaced by a numerical flux which will be discussed in the next section. Both the Hermite interpolation approximation of the function $\mathbf{U}$ and its derivative $\mathbf{S}$ are needed in the finite volume scheme. The procedures of FV hybrid Hermite WENO reconstruction of $\mathbf{U}^{\pm}(G_{s\ell},t)$ can be found in [32] and the reconstructions of its derivatives $\mathbf{S}$ are given in Appendix A. Let $\overline{\mathcal{U}}_K=\int_K\mathbf{U}(x,t)\phi(x)dx$ and $\mathcal{L}(\mathbf{U},\mathbf{S})_K=-\int_{\partial K}(\mathbf{F}\cdot\mathbf{n})\phi(x)ds+\int_K(\mathbf{F}\cdot\nabla\phi)dx$, the semi-discrete HWENO scheme (2.3) can be written as:

$$\frac{\mathrm{d}}{\mathrm{d}t}\overline{\mathcal{U}}_K=\mathcal{L}(\mathbf{U},\mathbf{S})_K. \tag{2.5}$$

The ODE (2.5) is discretized in time by the third order strong stability preserving (SSP) Runge-Kutta method:

$$\begin{cases}\overline{\mathcal{U}}_K^{(1)} &= \overline{\mathcal{U}}_K^n+\Delta t\mathcal{L}(\overline{\mathcal{U}}_K^n)\\ \overline{\mathcal{U}}_K^{(2)} &= \frac{3}{4}\overline{\mathcal{U}}_K^n+\frac{1}{4}(\overline{\mathcal{U}}_K^{(1)}+\Delta t\mathcal{L}(\overline{\mathcal{U}}_K^{(1)}))\\ \overline{\mathcal{U}}_K^{n+1} &= \frac{1}{3}\overline{\mathcal{U}}_K^n+\frac{2}{3}(\overline{\mathcal{U}}_K^{(2)}+\Delta t\mathcal{L}(\overline{\mathcal{U}}_K^{(2)}))\end{cases} \tag{2.6}$$

3. A positivity-preserving high order finite volume hybrid HWENO scheme

In this section, we construct a positivity-preserving high order finite volume hybrid HWENO scheme for solving compressible Navier-Stokes equations by combining the hybrid Hermite WENO schemes in [32] with the positivity-preserving high order method in [26].

3.1. One-dimensional case

Consider the one-dimensional dimensionless compressible Navier-Stokes equation in conservative form

$$\mathbf{U}_t+\mathbf{F}(\mathbf{U},\mathbf{S})_x=\mathbf{0}, \tag{3.1}$$

where $\mathbf{U}=(\rho,m,E)^T$ are the conservative variables and the superscript T denotes transpose of a vector. The flux function $\mathbf{F}(\mathbf{U},\mathbf{S})=\mathbf{F}^a-\mathbf{F}^d$ with $\mathbf{S}=\mathbf{U}_x$, and advection and diffusion fluxes are given respectively as $\mathbf{F}^a=\left(\rho u,\rho u^2+p,(E+p)u\right)^T$, $\mathbf{F}^d=(0,\tau,u\tau-q)^T$, where $\tau=\frac{\eta}{\mathrm{Re}}u_x$ is the shear stress tensor and $q=-\frac{\gamma}{\mathrm{Pr}\cdot\mathrm{Re}}e_x$ denotes the heat diffusion flux with $e=E/\rho-u^2/2$, $p=(\gamma-1)\rho e$, where ρ is the density, $m=\rho u$ is the momentum, u denotes the velocity, E is the total energy, e denotes the internal energy, p is the pressure, Re, γ and Pr are positive constants and $\eta=4/3$.

The test function $\phi(x)$ is taken $\frac{1}{\Delta x}$ and $\frac{x-x_i}{(\Delta x)^2}$ and the cell K is the interval $I_i=[x_{i-\frac{1}{2}},x_{i+\frac{1}{2}}]$ in (2.3) in one-dimensional case, then the semi-discrete hybrid HWENO scheme (2.5) can be written as

$$\begin{cases}\dfrac{\mathrm{d}\overline{\mathbf{U}}_i(t)}{\mathrm{d}t}=-\dfrac{1}{\Delta x}\left[\mathbf{F}(\mathbf{U},\mathbf{S})\,|_{x_{i+\frac{1}{2}},t}-\mathbf{F}(\mathbf{U},\mathbf{S})\,|_{x_{i-\frac{1}{2}},t}\right],\\ \dfrac{\mathrm{d}\overline{\mathbf{V}}_i(t)}{\mathrm{d}t}=-\dfrac{1}{2\Delta x}\left[\mathbf{F}(\mathbf{U},\mathbf{S})\,|_{x_{i+\frac{1}{2}},t}+\mathbf{F}(\mathbf{U},\mathbf{S})\,|_{x_{i-\frac{1}{2}},t}\right]+\dfrac{1}{(\Delta x)^2}\displaystyle\int_{I_i}\mathbf{F}(\mathbf{U},\mathbf{S})dx,\end{cases} \tag{3.2}$$

where the zeroth-order moment $\overline{\mathbf{U}}_i(t)=\frac{1}{\Delta x}\int_{I_i}\mathbf{U}(x,t)dx$ and the first order moment $\overline{\mathbf{V}}_i(t)=\frac{1}{\Delta x}\int_{I_i}\frac{x-x_i}{\Delta x}\mathbf{U}(x,t)dx$ in I_i. After replacing the flux function at the interface of cell I_i by the numerical flux, and using the Gauss-Lobatto quadrature to approximate the integral $\int_{I_i}\mathbf{F}(\mathbf{U},\mathbf{S})dx$, we can obtain the first order Euler forward time discretization finite volume hybrid HWENO scheme

$$\begin{cases}\overline{\mathbf{U}}_i^{n+1}=\overline{\mathbf{U}}_i^{n}-\dfrac{\Delta t}{\Delta x}(\widehat{\mathbf{F}}_{i+\frac{1}{2}}-\widehat{\mathbf{F}}_{i-\frac{1}{2}}),\\ \overline{\mathbf{V}}_i^{n+1}=\overline{\mathbf{V}}_i^{n}-\dfrac{\Delta t}{2\Delta x}(\widehat{\mathbf{F}}_{i+\frac{1}{2}}+\widehat{\mathbf{F}}_{i-\frac{1}{2}})+\dfrac{\Delta t}{\Delta x}\mathbf{F}_i,\end{cases}\tag{3.3}$$

where $\widehat{\mathbf{F}}_{i+\frac{1}{2}}$ is the numerical flux to approximate the value of the flux $\mathbf{F}(\mathbf{U},\mathbf{S})$ at the interface point $x_{i+\frac{1}{2}}$. We use the positivity-preserving numerical flux in [26] defined by

$$\begin{aligned}\widehat{\mathbf{F}}_{i+\frac{1}{2}}=&\widehat{\mathbf{F}}\left(\mathbf{U}^-_{i+\frac{1}{2}},\mathbf{S}^-_{i+\frac{1}{2}},\mathbf{U}^+_{i+\frac{1}{2}},\mathbf{S}^+_{i+\frac{1}{2}}\right)\\ =&\frac{1}{2}\left[\mathbf{F}\left(\mathbf{U}^-_{i+\frac{1}{2}},\mathbf{S}^-_{i+\frac{1}{2}}\right)+\mathbf{F}\left(\mathbf{U}^+_{i+\frac{1}{2}},\mathbf{S}^+_{i+\frac{1}{2}}\right)-\beta_{i+\frac{1}{2}}\left(\mathbf{U}^+_{i+\frac{1}{2}}-\mathbf{U}^-_{i+\frac{1}{2}}\right)\right]\end{aligned}\tag{3.4}$$

$$\beta_{i+\frac{1}{2}}>\max_{\mathbf{U}^{\pm}_{i+\frac{1}{2}},\mathbf{S}^{\pm}_{i+\frac{1}{2}}}\left[|u|+\frac{1}{2\rho^2 e}(\sqrt{\rho^2q^2+2\rho^2e|\tau-p|^2}+\rho|q|)\right]\tag{3.5}$$

and $\mathbf{F}_i$ is approximated by a four-point Gauss-Lobatto quadrature formula

$$\mathbf{F}_i=\frac{1}{\Delta x}\int_{I_i}\mathbf{F}(\mathbf{U},\mathbf{S}))dx\approx\sum_{\alpha=1}^{4}\hat{\omega}_\alpha\mathbf{F}(\mathbf{U}(\widehat{x}_i^\alpha,t),\mathbf{S}(\widehat{x}_i^\alpha,t)),\tag{3.6}$$

where the weights are $\widehat{\omega}_1=\widehat{\omega}_4=\frac{1}{12}$ and $\widehat{\omega}_2=\widehat{\omega}_3=\frac{5}{12}$, and the Gauss-Lobatto quadrature points on the cell I_i are $\widehat{x}_i^1=x_{i-\frac{1}{2}},\widehat{x}_i^2=x_{i-\frac{\sqrt{5}}{10}},\widehat{x}_i^3=x_{i+\frac{\sqrt{5}}{10}},\widehat{x}_i^4=x_{i+\frac{1}{2}}$ with $x_{i+a}=x_i+a\Delta x$.

Our goal is to design the conservative schemes that are positivity-preserving of density and internal energy or pressure. Here we consider the positivity of internal energy instead of pressure. For ideal gas, the equation of state is $p=(\gamma-1)\rho e$ which satisfies $p>0\Leftrightarrow e>0$ under the density $\rho>0$. So if the density $\rho>0$, positivity of pressure is equivalent to positivity of internal energy, which is also mentioned in [26]. However, the other equation of state does not have this conclusion such as Jones-Wilkins-Lee (JWL) equation of state for explosive products in [6]. Define the set of admissible states by

$$G=\left\{\mathbf{U}=\begin{pmatrix}\rho\\ m\\ E\end{pmatrix}:\rho>0,\quad \rho e(\mathbf{U})=(\gamma-1)(E-\frac{1}{2}\frac{m^2}{\rho})>0\right\}.\tag{3.7}$$

It is straightforward to check that ρe is a concave function of $\mathbf{U}$ if $\rho>0$. Thus it satisfies the Jensen's inequality: $\forall\mathbf{U}_1,\mathbf{U}_2\in G$, $\forall\lambda_1,\lambda_2\geq 0,\lambda_1+\lambda_2=1$,

$$\rho e(\lambda_1\mathbf{U}_1+\lambda_2\mathbf{U}_2)\geq\lambda_1\rho e(\mathbf{U}_1)+\lambda_2\rho e(\mathbf{U}_2).\tag{3.8}$$

Therefore, G is a convex set. Let $N=\lceil(k+3)/2\rceil$, namely, N is smallest integer satisfying $2N-3\geq k$ and k the degree of reconstruction polynomial. So a N-point Legendre Gauss-Lobatto quadrature formula on the interval $I_i=\left[x_{i-\frac{1}{2}},x_{i+\frac{1}{2}}\right]$ is exact for integrals of polynomials of degree up to $2N-3$. Denote these quadrature points as $\{\widehat{x}_i^\alpha:\alpha=1,2,...,N\}=\{x_{i-\frac{1}{2}}=\widehat{x}_i^1,\widehat{x}_i^2,\cdots,\widehat{x}_i^{N-1},\widehat{x}_i^N=x_{i+\frac{1}{2}}\}$ and let $\widehat{\omega}_\alpha$ be the normalized quadrature weights on the interval $[-\frac{1}{2},\frac{1}{2}]$ such that $\sum_{\mu=1}^{N}\widehat{\omega}_\alpha=1$. Let $\mathbf{P}_i(x)=(\rho_i(x),m_i(x),E_i(x))^T$ be the reconstruction polynomials of degree k in the scheme (3.3) on the interval I_i with cell average $\overline{\mathbf{U}}_i^n$ and nodal values $\mathbf{U}^-_{i+\frac{1}{2}}$ and $\mathbf{U}^+_{i-\frac{1}{2}}$ at two endpoints of the cell I_i, then

$$\overline{\mathbf{U}}_i^n=\frac{1}{\Delta x}\int_{I_i}\mathbf{P}_i(x)dx=\sum_{\alpha=1}^{N}\widehat{\omega}_\alpha\mathbf{P}_i\left(\widehat{x}_i^\alpha\right)=\sum_{\alpha=2}^{N-1}\widehat{\omega}_\alpha\mathbf{P}_i\left(\widehat{x}_i^\alpha\right)+\widehat{\omega}_1\mathbf{U}^+_{i-\frac{1}{2}}+\widehat{\omega}_N\mathbf{U}^-_{i+\frac{1}{2}}.\tag{3.9}$$

By the mean value theorem for (3.9), there exist some points x_i^1,x_i^2,x_i^3, in cell I_i such that

$$\left(\rho_i(x_i^1),m_i(x_i^2),E_i(x_i^3)\right)^T=\sum_{\alpha=2}^{N-1}\frac{\widehat{\omega}_\alpha}{1-\widehat{\omega}_1-\widehat{\omega}_N}\mathbf{P}_i\left(\widehat{x}_i^\alpha\right)=\frac{\overline{\mathbf{U}}_i^n-\widehat{\omega}_1\mathbf{U}^+_{i-\frac{1}{2}}-\widehat{\omega}_N\mathbf{U}^-_{i+\frac{1}{2}}}{1-\widehat{\omega}_1-\widehat{\omega}_N}.\tag{3.10}$$

Then we have the following sufficient condition for positivity of cell averages, which can be easily enforced to preserve positivity of density and pressure without constructing the polynomials $\mathbf{P}_i(x)$.

Theorem 1. *A sufficient condition for $\overline{\mathbf{U}}_i^{n+1} \in G$ in the scheme (3.3) with reconstruction polynomials $\mathbf{P}_i(x) = (\rho_i(x), m_i(x), E_i(x))^T$ of degree k is*

$$\mathbf{U}^{\pm}_{i\pm\frac{1}{2}} \in G, \quad \frac{\overline{\mathbf{U}}_i^n - \hat{\omega}_1 \mathbf{U}^{+}_{i-\frac{1}{2}} - \hat{\omega}_N \mathbf{U}^{-}_{i+\frac{1}{2}}}{1-\hat{\omega}_1-\hat{\omega}_N} \in G, \quad \forall i \tag{3.11}$$

under the CFL condition

$$\frac{\Delta t}{\Delta x}\max_i \beta_{i+\frac{1}{2}} \le \widehat{\omega} = \frac{1}{N(N-1)}, \quad N = \lceil (k+3)/2 \rceil \tag{3.12}$$

where $\widehat{\omega}$ denote the smallest weight in $\widehat{\omega}_\alpha$, i.e., $\widehat{\omega} = \widehat{\omega}_1 = \widehat{\omega}_N$.

Proof. By plugging (3.4), (3.9) and (3.10) into the first equation of scheme (3.3), we obtain

$$\begin{aligned}
\overline{\mathbf{U}}_i^{n+1} =& \left(\widehat{\omega}_1 - \frac{1}{2}\frac{\Delta t}{\Delta x}\beta_{i-\frac{1}{2}}\right)\left[\mathbf{U}^{+}_{i-\frac{1}{2}} + \frac{1}{2}\frac{\Delta t}{\Delta x}\left(\widehat{\omega}_1 - \frac{1}{2}\frac{\Delta t}{\Delta x}\beta_{i-\frac{1}{2}}\right)^{-1}\mathbf{F}\left(\mathbf{U}^{+}_{i-\frac{1}{2}}, \mathbf{S}^{+}_{i-\frac{1}{2}}\right)\right] \\
&+ \left(\widehat{\omega}_N - \frac{1}{2}\frac{\Delta t}{\Delta x}\beta_{i+\frac{1}{2}}\right)\left[\mathbf{U}^{-}_{i+\frac{1}{2}} - \frac{1}{2}\frac{\Delta t}{\Delta x}\left(\widehat{\omega}_N - \frac{1}{2}\frac{\Delta t}{\Delta x}\beta_{i+\frac{1}{2}}\right)^{-1}\mathbf{F}\left(\mathbf{U}^{-}_{i+\frac{1}{2}}, \mathbf{S}^{-}_{i+\frac{1}{2}}\right)\right] \\
&+ \frac{1}{2}\frac{\Delta t}{\Delta x}\beta_{i-\frac{1}{2}}\left[\mathbf{U}^{-}_{i-\frac{1}{2}} + \beta^{-1}_{i-\frac{1}{2}}\mathbf{F}\left(\mathbf{U}^{-}_{i-\frac{1}{2}}, \mathbf{S}^{-}_{i-\frac{1}{2}}\right)\right] + \frac{1}{2}\frac{\Delta t}{\Delta x}\beta_{i+\frac{1}{2}}\left[\mathbf{U}^{+}_{i+\frac{1}{2}} - \beta^{-1}_{i+\frac{1}{2}}\mathbf{F}\left(\mathbf{U}^{+}_{i+\frac{1}{2}}, \mathbf{S}^{+}_{i+\frac{1}{2}}\right)\right] \\
&+ (1-\widehat{\omega}_1-\widehat{\omega}_N)\frac{\overline{\mathbf{U}}_i^n - \widehat{\omega}_1\mathbf{U}^{+}_{i-\frac{1}{2}} - \widehat{\omega}_N\mathbf{U}^{-}_{i+\frac{1}{2}}}{1-\widehat{\omega}_1-\widehat{\omega}_N}.
\end{aligned} \tag{3.13}$$

First we set

$$\beta_{i+\frac{1}{2}} > \max_{\mathbf{U}^{-}_{i+\frac{1}{2}}, \mathbf{S}^{-}_{i+\frac{1}{2}}, \mathbf{U}^{+}_{i+\frac{1}{2}}\mathbf{S}^{+}_{i+\frac{1}{2}}} \left[|u| + \frac{1}{2\rho^2 e}\left(\sqrt{\rho^2 q^2 + 2\rho^2 e|\tau - p|^2} + \rho|q|\right)\right].$$

Then under the CFL condition $\frac{\Delta t}{\Delta x}\max_i \beta_{i+\frac{1}{2}} \le \widehat{\omega}$, we have $\frac{1}{2}\frac{\Delta t}{\Delta x}\left(\widehat{\omega} - \frac{1}{2}\frac{\Delta t}{\Delta x}\beta_{i+\frac{1}{2}}\right)^{-1} \le \beta^{-1}_{i+\frac{1}{2}}$. By the Lemma 6 in [26], we have

$$\begin{aligned}
&\mathbf{U}^{-}_{i-\frac{1}{2}} \in G \Rightarrow \mathbf{U}^{-}_{i-\frac{1}{2}} + \beta^{-1}_{i-\frac{1}{2}}\mathbf{F}\left(\mathbf{U}^{-}_{i-\frac{1}{2}}, \mathbf{S}^{-}_{i-\frac{1}{2}}\right) \in G, \\
&\mathbf{U}^{+}_{i+\frac{1}{2}} \in G \Rightarrow \mathbf{U}^{+}_{i+\frac{1}{2}} - \beta^{-1}_{i+\frac{1}{2}}\mathbf{F}\left(\mathbf{U}^{+}_{i+\frac{1}{2}}, \mathbf{S}^{+}_{i+\frac{1}{2}}\right) \in G, \\
&\mathbf{U}^{+}_{i-\frac{1}{2}} \in G \Rightarrow \mathbf{U}^{+}_{i-\frac{1}{2}} + \frac{1}{2}\frac{\Delta t}{\Delta x}\left(\widehat{\omega}_1 - \frac{1}{2}\frac{\Delta t}{\Delta x}\beta_{i-\frac{1}{2}}\right)^{-1}\mathbf{F}\left(\mathbf{U}^{+}_{i-\frac{1}{2}}, \mathbf{S}^{+}_{i-\frac{1}{2}}\right) \in G, \\
&\mathbf{U}^{-}_{i+\frac{1}{2}} \in G \Rightarrow \mathbf{U}^{-}_{i+\frac{1}{2}} - \frac{1}{2}\frac{\Delta t}{\Delta x}\left(\widehat{\omega}_N - \frac{1}{2}\frac{\Delta t}{\Delta x}\beta_{i+\frac{1}{2}}\right)^{-1}\mathbf{F}\left(\mathbf{U}^{-}_{i+\frac{1}{2}}, \mathbf{S}^{-}_{i+\frac{1}{2}}\right) \in G.
\end{aligned}$$

Moreover, (3.13) is a convex combination under the same CFL condition (3.12). Thus we get $\overline{\mathbf{U}}_i^{n+1} \in G$ for the scheme (3.3). □

To enforce the condition (3.12) in Theorem 1, we use the simplified scaling limiter for HWENO schemes in [29]. For convenience, assume there is a vector of reconstructed polynomials $\mathbf{P}_i(x) = (\rho_i(x), m_i(x), E_i(x))^T$ on the interval I_i with the cell average $\overline{\mathbf{P}}_i = \left(\overline{\rho}_i, \overline{m}_i, \overline{E}_i\right)^T$. Define $\overline{\rho e}_i = \rho e(\overline{\mathbf{P}}_i) = \overline{E}_i - \frac{1}{2}\overline{m}_i^2/\overline{\rho}_i$. Assume $\overline{\mathbf{P}}_i$ has positive density and energy, i.e., $\overline{\rho}_i > 0$, $\overline{E}_i > 0$. We seek polynomials $\widetilde{\mathbf{P}}_i(x)$ with the same cell averages so that $\widetilde{\mathbf{P}}_i(\widehat{x}_i^1)$, $\widetilde{\mathbf{P}}_i(\widehat{x}_i^N)$, $\sum_{\alpha=2}^{N-1}\frac{\widehat{\omega}_\alpha}{1-2\widehat{\omega}}\widetilde{\mathbf{P}}_i(\widehat{x}_i^\alpha) \in G$. The following procedure can be applied to enforce the sufficient condition (3.11) for each cell I_i:

1. To keep the positivity of density, we modify firstly density by

$$\widehat{\rho}_i(x) = \theta_\rho\left(\rho_i(x) - \bar{\rho}_i\right) + \bar{\rho}_i, \quad \theta_\rho = \min\left\{1, \frac{\bar{\rho}_i - \varepsilon}{\bar{\rho}_i - \rho_{min}}\right\} \tag{3.14}$$

where ε is a small positive number as the desired lower bound for density, e.g., $\varepsilon = 10^{-13}$, $\rho_{min} = \min\{\rho_i(\widehat{x}_i^1), \rho_i(\widehat{x}_i^N), \rho_i(\widehat{x}_i^*)\}$ with $\rho_i(\widehat{x}_i^*) = \frac{1}{1-2\widehat{\omega}}(\bar{\rho}_i - \widehat{\omega}_1\rho_i(\widehat{x}_i^1) - \widehat{\omega}_N\rho_i(\widehat{x}_i^N))$ and $\theta_\rho \in [0,1]$. Since $\bar{\rho}_i = \widehat{\omega}\rho_i(\widehat{x}_i^1) + \widehat{\omega}\rho_i(\widehat{x}_i^1) + (1-2\omega)\rho_i(x_i^*)$, we have

$\bar{\rho}_i \geq \min\{\rho_i(\widehat{x}_i^1), \rho_i(\widehat{x}_i^N), \rho_i(\widehat{x}_i^*)\}$, thus $\theta_\rho \in [0,1]$. Moreover, it's straightforward to check that $\rho_i(\widehat{x}_i^1) > 0$, $\rho_i(\widehat{x}_i^N) > 0$ and $\widehat{\rho}_i(x_i^*) \geq 0$. Then $\widehat{\rho}^-_{i+\frac{1}{2}} = \theta_\rho\left(\rho^-_{i+\frac{1}{2}} - \bar{\rho}_i\right) + \bar{\rho}_i$, $\widehat{\rho}^+_{i-\frac{1}{2}} = \theta_\rho\left(\rho^+_{i-\frac{1}{2}} - \bar{\rho}_i\right) + \bar{\rho}_i$.

Let $\widehat{\mathbf{P}}_i(x) = (\widehat{\rho}_i(x), m_i(x), E_i(x))^T$. The convex combination $\sum_{\alpha=2}^{N-1} \frac{1}{1-2\widehat{\omega}} \widehat{\mathbf{P}}_i(\widehat{x}_i^\alpha)$ is equal to $(\widehat{\rho}_i(x_i^{*,1}), \widehat{m}_i(x_i^{*,2}), \widehat{E}_i(x_i^{*,3}))^T$ by the mean value theorem, where x_i^{*1}, x_i^{*2}, x_i^{*3} are three different points on the cell I_i. We abuse the notation by using $\widehat{\mathbf{P}}_i(x_i^{**})$ to denote the vector $(\widehat{\rho}_i(x_i^{*,1}), \widehat{m}_i(x_i^{*,2}), \widehat{E}_i(x_i^{*,3}))^T$, then $\widehat{\mathbf{P}}_i(x_i^{**}) = \frac{1}{1-2\widehat{\omega}}(\overline{\mathbf{P}}_i - \widehat{\omega}_1\widehat{\mathbf{P}}_i(\widehat{x}_i^1) - \widehat{\omega}_N\widehat{\mathbf{P}}_i(\widehat{x}_i^N))$.

2. For enforcing the positivity of internal energy, we perform the following procedure

$$\widetilde{\mathbf{P}}_i(x) = \theta_e\left(\widehat{\mathbf{P}}_i(x) - \overline{\mathbf{P}}_i\right) + \overline{\mathbf{P}}_i, \quad \theta_e = \min\left\{1, \frac{\overline{\rho e}_i - \varepsilon}{\overline{\rho e}_i - \rho e_{min}}\right\}, \tag{3.15}$$

where ε is a small positive number as the desired lower bound for internal energy, e.g., $\varepsilon = 10^{-13}$, $\rho e_{min} = \min\left\{\rho e(\widehat{\mathbf{P}}_i(\widehat{x}_i^1)), \rho e(\widehat{\mathbf{P}}_i(\widehat{x}_i^N))\rho e(\widehat{\mathbf{P}}_i(\widehat{x}_i^{**}))\right\}$ and $\theta_e \in [0,1]$. Since the cell average of $\widehat{\mathbf{P}}_i(x)$ is still $\overline{\mathbf{P}}_i$, we have the convex combination $\overline{\mathbf{P}}_i = \widehat{\omega}_1\widehat{\mathbf{P}}_i(\widehat{x}_i^1) + \widehat{\omega}_N\widehat{\mathbf{P}}_i(\widehat{x}_i^N) + (1-2\widehat{\omega})\widehat{\mathbf{P}}_i(x_i^{**})$, so $\rho e(\overline{\mathbf{P}}_i) \geq \widehat{\omega}_1\rho e\left(\widehat{\mathbf{P}}_i(\widehat{x}_i^1)\right) + \widehat{\omega}_N\rho e\left(\widehat{\mathbf{P}}_i(\widehat{x}_i^N)\right) + (1-2\widehat{\omega})\rho e\left(\widehat{\mathbf{P}}_i(x_i^{**})\right)$ by the Jensen's inequality, thus $\theta_e \in [0,1]$. It's straightforward to check $\widetilde{\mathbf{P}}_i(\widehat{x}_i^1), \widetilde{\mathbf{P}}_i(\widehat{x}_i^N) \in G$ and $\widetilde{\mathbf{P}}_i(x_i^{**}) \in G$. Therefore, we get the polynomial $\widetilde{\mathbf{P}}_i(x)$ satisfying the condition (3.11).

In fact, we only need to obtain the point values $\widetilde{\mathbf{U}}^\pm_{i\mp\frac{1}{2}} = \widetilde{\mathbf{P}}_i(x_{j\mp\frac{1}{2}})$ in a finite volume scheme. For simplicity, denote $\widehat{\mathbf{q}}_i^1 = \widehat{\mathbf{P}}^-_{i+\frac{1}{2}} = (\widehat{\rho}^-_{i+\frac{1}{2}}, m^-_{i+\frac{1}{2}}, E^-_{i+\frac{1}{2}})^T$, $\widehat{\mathbf{q}}_i^2 = \widehat{\mathbf{P}}^+_{i-\frac{1}{2}} = (\widehat{\rho}^+_{i-\frac{1}{2}}, m^+_{i-\frac{1}{2}}, E^+_{i-\frac{1}{2}})^T$ and $\widehat{\mathbf{q}}_i^3 = \frac{\bar{\mathbf{P}}_i - \hat{\omega}\widehat{\mathbf{P}}^+_{i-\frac{1}{2}} - \hat{\omega}\widehat{\mathbf{P}}^-_{i+\frac{1}{2}}}{1-2\hat{\omega}}$. For $k = 1,2,3$, if $\rho e(\widehat{\mathbf{q}}^k) < \varepsilon$, then set $t_\varepsilon^k = \frac{\rho e(\widehat{\mathbf{q}}^k) - \varepsilon}{\rho e(\bar{\mathbf{P}}_i) - \rho e(\widehat{\mathbf{q}}^k)}$; if $\rho e(\widehat{\mathbf{q}}^k) \geq \varepsilon$, then set $t_\varepsilon^k = 1$. Take $\theta_e = \min\{t_\varepsilon^1, t_\varepsilon^2, t_\varepsilon^3\}$, then

$$\widetilde{\mathbf{U}}^+_{i-\frac{1}{2}} = \widetilde{\mathbf{P}}_i(x_{i-\frac{1}{2}}) = \theta_e\left(\widehat{\mathbf{P}}^+_{i-\frac{1}{2}} - \overline{\mathbf{P}}_i\right) + \overline{\mathbf{P}}_i,$$

$$\widetilde{\mathbf{U}}^-_{i+\frac{1}{2}} = \widetilde{\mathbf{P}}_i(x_{i+\frac{1}{2}}) = \theta_e\left(\widehat{\mathbf{P}}^-_{i+\frac{1}{2}} - \overline{\mathbf{P}}_i\right) + \overline{\mathbf{P}}_i.$$

Finally, use $\widetilde{\mathbf{U}}^+_{i-\frac{1}{2}}, \widetilde{\mathbf{U}}^-_{i+\frac{1}{2}}$ instead of $\mathbf{U}^+_{i-\frac{1}{2}}, \mathbf{U}^-_{i+\frac{1}{2}}$ in the scheme (3.3).

Remark 3.1. It is needed to emphasize that we mainly introduce the design and implementation of positivity-preserving property of one-dimensional FV hybrid HWENO scheme. $\overline{\mathbf{U}}_i^n$ and $\overline{\mathbf{V}}_i^n$ in (3.2) are applied to HWENO interpolation for the approximation of the function $\mathbf{U}$ and its derivative $\mathbf{S}$ in Gauss-Labotto points, and the detailed procedures of FV hybrid HWENO interpolation in one dimensional case are given in the appendix A.

Remark 3.2. To obtain processed point value $\widetilde{\mathbf{U}}^\pm_{i\mp\frac{1}{2}}$, we only need cell average $\overline{\mathbf{U}}_i$ and point values $\mathbf{U}^\pm_{i\mp\frac{1}{2}}, \mathbf{U}^\pm_{i\mp\frac{1}{2}}$ in the limiter (3.14) and (3.15). The reconstruction polynomials $\mathbf{P}_i(x)$ are not needed in implementation. It is a high order accurate and conservative limiter [26].

3.2. Two-dimensional case

Consider the two-dimensional dimensionless compressible Navier-Stokes equation in conservative form

$$\mathbf{U}_t + \nabla\cdot\mathbf{F}(\mathbf{U},\mathbf{S}) = 0 \tag{3.16}$$

where $\mathbf{U} = (\rho, \rho\mathbf{u}, E)^T$ are the conservative variables with the velocity $\mathbf{u} = (u,v)$, $\mathbf{S} = \nabla\mathbf{U}$ and the flux function $\mathbf{F}(\mathbf{U},\mathbf{S}) = \mathbf{F}^a - \mathbf{F}^d$ with advection and diffusion fluxes as

$$\mathbf{F}^a = \begin{pmatrix} \rho\mathbf{U} \\ \rho\mathbf{U}\otimes\mathbf{U} + p\mathbb{I} \\ (E+p)\mathbf{U} \end{pmatrix}, \quad \mathbf{F}^d = \begin{pmatrix} 0 \\ \boldsymbol{\tau} \\ \mathbf{u}\cdot\boldsymbol{\tau} - \mathbf{q} \end{pmatrix}, \tag{3.17}$$

where ρ is the density, m and n are the momentas given by $m = \rho u$ and $n = \rho v$, u and v denotes the velocity, E is the total energy, e denotes the internal energy, p is the pressure and $\mathbb{I}$ is the unit tensor. The shear stress tensor and heat diffusion flux are

$$\boldsymbol{\tau} = \frac{1}{\mathrm{Re}}\begin{pmatrix} \tau_{xx} & \tau_{xy} \\ \tau_{yx} & \tau_{yy} \end{pmatrix}, \quad \mathbf{q} = \frac{1}{\mathrm{Re}}\frac{\gamma}{\mathrm{Pr}}(e_x, e_y)^T \tag{3.18}$$

with

$$e = \frac{E}{\rho} - \frac{1}{2}(u^2+v^2), \quad p = (\gamma-1)\rho e \tag{3.19}$$

and

$$\tau_{xx} = \frac{4}{3}u_x - \frac{2}{3}v_y, \quad \tau_{xy} = \tau_{yx} = u_y + v_x, \quad \tau_{yy} = \frac{4}{3}v_y - \frac{2}{3}u_x.$$

The equation (3.16) can be written as

$$\mathbf{U}_t + \mathbf{F}(\mathbf{U},\mathbf{S})_x + \mathbf{G}(\mathbf{U},\mathbf{S})_y = 0 \tag{3.20}$$

with

$$\mathbf{F}(\mathbf{U},\mathbf{S}) = \begin{pmatrix} \rho u \\ \rho u^2 + p - \frac{\tau_{xx}}{\mathrm{Re}} \\ \rho uv - \frac{\tau_{yx}}{\mathrm{Re}} \\ (E+p)u - \frac{1}{\mathrm{Re}}(\tau_{xx}u + \tau_{yx}v + \frac{\gamma}{\mathrm{Pr}}e_x) \end{pmatrix},$$

$$\mathbf{G}(\mathbf{U},\mathbf{S}) = \begin{pmatrix} \rho v \\ \rho uv - \frac{\tau_{xy}}{\mathrm{Re}} \\ \rho v^2 + p - \frac{\tau_{yy}}{\mathrm{Re}} \\ (E+p)v - \frac{1}{\mathrm{Re}}(\tau_{xy}u + \tau_{yy}v + \frac{\gamma}{\mathrm{Pr}}e_y) \end{pmatrix}.$$

The test function $\phi(x,y)$ is taken as $\frac{1}{\Delta x\Delta y}$, $\frac{x-x_i}{(\Delta x)^2\Delta y}$ and $\frac{y-y_j}{\Delta x(\Delta y)^2}$ and cell K is a rectangular $[x_{i-\frac{1}{2}}, x_{i+\frac{1}{2}}] \times [y_{j-\frac{1}{2}}, y_{j+\frac{1}{2}}]$ in (2.3) in two-dimensional case. Then the semi-discrete hybrid HWENO scheme (2.5) can be written as

$$\begin{cases}
\dfrac{d\overline{\mathbf{U}}_{ij}(t)}{dt} = -\dfrac{1}{\Delta x\Delta y}\displaystyle\int_{y_{j-\frac{1}{2}}}^{y_{j+\frac{1}{2}}}\left[\mathbf{F}(\mathbf{U},\mathbf{S})\,|_{x_{i+\frac{1}{2}},y} - \mathbf{F}(\mathbf{U},\mathbf{S})\,|_{x_{i-\frac{1}{2}},y}\right]dy \\
\qquad\qquad -\dfrac{1}{\Delta x\Delta y}\displaystyle\int_{x_{i-\frac{1}{2}}}^{x_{i+\frac{1}{2}}}\left[\mathbf{G}(\mathbf{U},\mathbf{S})\,|_{x,y_{j+\frac{1}{2}}} - \mathbf{G}(\mathbf{U},\mathbf{S})\,|_{x,y_{j-\frac{1}{2}}}\right]dx, \\
\dfrac{d\overline{\mathbf{V}}_{ij}(t)}{dt} = -\dfrac{1}{2\Delta x\Delta y}\displaystyle\int_{y_{j-\frac{1}{2}}}^{y_{j+\frac{1}{2}}}\left[\mathbf{F}(\mathbf{U},\mathbf{S})\,|_{x_{i-\frac{1}{2}},y} + \mathbf{F}(\mathbf{U},\mathbf{S})\,|_{x_{i+\frac{1}{2}},y}\right]dy \\
\qquad\qquad -\dfrac{1}{\Delta x\Delta y}\displaystyle\int_{x_{i-\frac{1}{2}}}^{x_{i+\frac{1}{2}}}\dfrac{x-x_i}{\Delta x}\left[\mathbf{G}(\mathbf{U},\mathbf{S})\,|_{x,y_{j+\frac{1}{2}}} - \mathbf{G}(\mathbf{U},\mathbf{S})\,|_{x,y_{j-\frac{1}{2}}}\right]dx \\
\qquad\qquad +\dfrac{1}{(\Delta x)^2\Delta y}\displaystyle\int_{x_{i-\frac{1}{2}}}^{x_{i+\frac{1}{2}}}\int_{y_{j-\frac{1}{2}}}^{y_{j+\frac{1}{2}}}\mathbf{F}(\mathbf{U},\mathbf{S})dxdy, \\
\dfrac{d\overline{\mathbf{W}}_{ij}(t)}{dt} = -\dfrac{1}{\Delta x\Delta y}\displaystyle\int_{y_{j-\frac{1}{2}}}^{y_{j+\frac{1}{2}}}\dfrac{y-y_j}{\Delta y}[\mathbf{F}(\mathbf{U},\mathbf{S})\,|_{x_{i+\frac{1}{2}},y} - \mathbf{F}(\mathbf{U},\mathbf{S})\,|_{x_{i-\frac{1}{2}},y}]dy \\
\qquad\qquad -\dfrac{1}{2\Delta x\Delta y}\displaystyle\int_{x_{i-\frac{1}{2}}}^{x_{i+\frac{1}{2}}}\left[\mathbf{G}(\mathbf{U},\mathbf{S})\,|_{x,y_{j-\frac{1}{2}}} + \mathbf{G}(\mathbf{U},\mathbf{S})\,|_{x,y_{j+\frac{1}{2}}}\right]dx \\
\qquad\qquad +\dfrac{1}{\Delta x(\Delta y)^2}\displaystyle\int_{x_{i-\frac{1}{2}}}^{x_{i+\frac{1}{2}}}\int_{y_{j-\frac{1}{2}}}^{y_{j+\frac{1}{2}}}\mathbf{G}(\mathbf{U},\mathbf{S})dxdy,
\end{cases} \tag{3.21}$$

where

$$\overline{\mathbf{U}}_{ij}(t) = \frac{1}{\Delta x \Delta y}\int_K \mathbf{U}(x, y, t)dxdy,$$
$$\overline{\mathbf{V}}_{ij}(t) = \frac{1}{\Delta x \Delta y}\int_K \mathbf{U}(x, y, t)\frac{x - x_i}{\Delta x}dxdy,$$
$$\overline{\mathbf{W}}_{ij}(t) = \frac{1}{\Delta x \Delta y}\int_K \mathbf{U}(x, y, t)\frac{y - y_j}{\Delta y}dxdy.$$

The integral in (3.21) can be approximated by quadrature with sufficient accuracy. Assume $\{x_i^\beta, \beta = 1, ..., L\}$ and $\{y_j^\beta, \beta = 1, ..., L\}$ denote the Gauss quadrature points on the interval $[x_{i-\frac{1}{2}}, x_{i+\frac{1}{2}}]$ and $[y_{j-\frac{1}{2}}, y_{j+\frac{1}{2}}]$ respectively, ω_β are the corresponding weights of the Gauss quadrature on interval $[-\frac{1}{2}, \frac{1}{2}]$ satisfing $\sum_{\beta=1}^L \omega_\beta = 1$. For example, $(x_{i-\frac{1}{2}}, y_j^\beta)$ are the Gauss quadrature points on the left edge of the cell I_{ij}, where the subscript β denotes the values at the Gauss quadrature points, for instance, $u^+_{i-\frac{1}{2},\beta} = u^+_{i-\frac{1}{2},j}(y_j^\beta)$. Denote $\lambda_1 = \frac{\Delta t}{\Delta x}$ and $\lambda_2 = \frac{\Delta t}{\Delta y}$. Using the numerical flux to approximate the value of the flux at the interface of the cell (i, j) and Gauss quadrature to approximate the integral terms in (3.21), then we can obtain the first order Euler forward time discretization finite volume hybrid HWENO scheme

$$\begin{cases}
\overline{\mathbf{U}}_{ij}^{n+1} = \overline{\mathbf{U}}_{ij}^{n} - \lambda_1 \sum_{\beta=1}^{L} \omega_\beta (\widehat{\mathbf{F}}_{i+\frac{1}{2},\beta} - \widehat{\mathbf{F}}_{i-\frac{1}{2},\beta}) - \lambda_2 \sum_{\beta=1}^{L} \omega_\beta (\widehat{\mathbf{G}}_{\beta,j+\frac{1}{2}} - \widehat{\mathbf{G}}_{\beta,j-\frac{1}{2}}) \\
\overline{\mathbf{V}}_{ij}^{n+1} = \overline{\mathbf{V}}_{ij}^{n} - \frac{\lambda_1}{2} \sum_{\beta=1}^{L} \omega_\beta (\widehat{\mathbf{F}}_{i+\frac{1}{2},\beta} + \widehat{\mathbf{F}}_{i-\frac{1}{2},\beta}) + \lambda_1 \sum_{\beta=1}^{L}\sum_{\gamma=1}^{L} \omega_k\omega_l \mathbf{F}\left(\mathbf{U}(x_i^\beta, y_j^\gamma), \mathbf{S}(x_i^\beta, y_j^\gamma)\right) \\
\qquad - \lambda_2 \sum_{\beta=1}^{L} \omega_\beta \frac{x_\beta - x_i}{\Delta x} (\widehat{\mathbf{G}}_{\beta,j+\frac{1}{2}} - \widehat{\mathbf{G}}_{\beta,j-\frac{1}{2}}) \\
\overline{\mathbf{W}}_{ij}^{n+1} = \overline{\mathbf{W}}_{ij}^{n} - \lambda_1 \sum_{\alpha=1}^{L} \omega_\beta \frac{y_\beta - y_j}{\Delta y} (\widehat{\mathbf{F}}_{i+\frac{1}{2},\beta} - \widehat{\mathbf{F}}_{i-\frac{1}{2},\beta}) - \frac{\lambda_2}{2} \sum_{\beta=1}^{L} \omega_\beta (\widehat{\mathbf{G}}_{\beta,j+\frac{1}{2}} + \widehat{\mathbf{G}}_{\beta,j-\frac{1}{2}}) \\
\qquad + \lambda_2 \sum_{\beta=1}^{L}\sum_{\gamma=1}^{L} \omega_\beta\omega_\gamma \mathbf{G}\left(\mathbf{U}(x_i^\beta, y_j^\gamma), \mathbf{S}(x_i^\beta, y_j^\gamma)\right),
\end{cases} \tag{3.22}$$

where $\widehat{\mathbf{F}}_{i+\frac{1}{2},\beta}$ and $\widehat{\mathbf{G}}_{\beta,j+\frac{1}{2}}$ are the numerical flux to approximate the value of the flux $\mathbf{F}(\mathbf{U}, \mathbf{S})$ and $\mathbf{G}(\mathbf{U}, \mathbf{S})$ at the point $(x_{i+\frac{1}{2}}, y_j^\beta)$ and $(x_i^\beta, y_{j+\frac{1}{2}})$ respectively, defined by

$$\begin{aligned}
\widehat{\mathbf{F}}_{i+\frac{1}{2},\beta} =& \widehat{\mathbf{F}}\left(\mathbf{U}^-_{i+\frac{1}{2},\beta}, \mathbf{S}^-_{i+\frac{1}{2},\beta}, \mathbf{U}^+_{i+\frac{1}{2},\beta}, \mathbf{S}^+_{i+\frac{1}{2},\beta}\right) \\
=& \frac{1}{2}\left[\mathbf{F}\left(\mathbf{U}^-_{i+\frac{1}{2},\beta}, \mathbf{S}^-_{i+\frac{1}{2},\beta}\right) + \mathbf{F}\left(\mathbf{U}^+_{i+\frac{1}{2},\beta}, \mathbf{S}^+_{i+\frac{1}{2},\beta}\right) - \beta_{i+\frac{1}{2}}\left(\mathbf{U}^+_{i+\frac{1}{2},\beta} - \mathbf{U}^-_{i+\frac{1}{2},\beta}\right)\right], \\
\beta_{i+\frac{1}{2}} >& \max_{\mathbf{U}^\pm_{i+\frac{1}{2},\beta}, \mathbf{S}^\pm_{i+\frac{1}{2},\beta}} \left[|\mathbf{u}\cdot\mathbf{n}_i| + \frac{1}{2\rho^2 e}\left(\sqrt{\rho^2 |\mathbf{q}\cdot\mathbf{n}_i|^2 + 2\rho^2 e \left\|\boldsymbol{\tau}\cdot\mathbf{n}_i - p\mathbf{n}_i^T\right\|^2} + \rho |\mathbf{q}\cdot\mathbf{n}_i|\right)\right],
\end{aligned} \tag{3.23}$$

$$\begin{aligned}
\widehat{\mathbf{G}}_{\beta,j+\frac{1}{2}} =& \widehat{\mathbf{G}}\left(\mathbf{U}^-_{\beta,j+\frac{1}{2}}, \mathbf{S}^-_{\beta,j+\frac{1}{2}}, \mathbf{U}^+_{\beta,j+\frac{1}{2}}, \mathbf{S}^+_{\beta,j+\frac{1}{2}}\right) \\
=& \frac{1}{2}\left[\mathbf{G}\left(\mathbf{U}^-_{\beta,j+\frac{1}{2}}, \mathbf{S}^-_{\beta,j+\frac{1}{2}}\right) + \mathbf{G}\left(\mathbf{U}^+_{\beta,j+\frac{1}{2}}, \mathbf{S}^+_{\beta,j+\frac{1}{2}}\right) - \beta_{j+\frac{1}{2}}\left(\mathbf{U}^+_{\beta,j+\frac{1}{2}} - \mathbf{U}^-_{\beta,j-\frac{1}{2}}\right)\right] \\
\beta_{j+\frac{1}{2}} >& \max_{\mathbf{U}^\pm_{\beta,j+\frac{1}{2}}, \mathbf{S}^\pm_{\beta,j+\frac{1}{2}}} \left[|\mathbf{u}\cdot\mathbf{n}_j| + \frac{1}{2\rho^2 e}\left(\sqrt{\rho^2 |\mathbf{q}\cdot\mathbf{n}_j|^2 + 2\rho^2 e \left\|\boldsymbol{\tau}\cdot\mathbf{n}_j - p\mathbf{n}_j^T\right\|^2} + \rho |\mathbf{q}\cdot\mathbf{n}_j|\right)\right]
\end{aligned} \tag{3.24}$$

with $\mathbf{n}_i = (1, 0)$ and $\mathbf{n}_j = (0, 1)$.

Our goal is to design the conservative schemes that are positivity-preserving of density and internal energy. Here we still consider the positivity of internal energy instead of pressure. Define the set of admissible states by

$$G=\left\{\mathbf{U}=\begin{pmatrix}\rho\\ m\\ n\\ E\end{pmatrix}:\rho>0,\quad \rho e(\mathbf{U})=E-\frac{1}{2}\frac{m^2+n^2}{\rho}>0\right\}. \tag{3.25}$$

We will use Gauss-Lobatto quadrature rule on (i,j) cell, denote $\{\hat{x}_i^\alpha,\alpha=1,...,N\}$ as the Gauss-Lobatto points on the interval $[x_{i-\frac{1}{2}},x_{i+\frac{1}{2}}]$ and $\{\hat{y}_j^\alpha,\alpha=1,...,N\}$ as the Gauss-Lobatto points on the interval $[y_{j-\frac{1}{2}},y_{j+\frac{1}{2}}]$. For simplicity, assume that we have a vector of approximation polynomials of degree k at time t, $\mathcal{H}_{ij}(x,y)=(\rho_{ij}(x,y),m_{ij}(x,y),n_{ij}(x,y),E_{ij}(x,y))^T$ with the cell average $\overline{\mathbf{U}}_{ij}^n=(\overline{\rho}_{ij},\overline{m}_{ij},\overline{n}_{ij},\overline{E}_{ij})^T$. Consider the quadrature rule for $\mathbf{U}_{ij}(x,y)$ on the rectangle $I_{ij}=[x_{i-\frac{1}{2}},x_{i+\frac{1}{2}}]\times[y_{j-\frac{1}{2}},y_{j+\frac{1}{2}}]$ with approximation polynomials $\mathcal{H}_{ij}(x,y)$. Denote $\mu_1=\frac{\lambda_1}{\lambda_1+\lambda_2}$, $\mu_2=\frac{\lambda_2}{\lambda_1+\lambda_2}$, then

$$\begin{aligned}\overline{\mathbf{U}}_{ij}^n&=\frac{\mu_1}{\Delta x\Delta y}\int_{I_{ij}}\mathcal{H}_{ij}(x,y)dxdy+\frac{\mu_2}{\Delta x\Delta y}\int_{I_{ij}}\mathcal{H}_{ij}(x,y)dxdy\\&=\mu_1\sum_{\beta=1}^{L}\sum_{\alpha=1}^{N}\omega_\beta\hat{\omega}_\alpha\mathcal{H}_{ij}(\hat{x}_i^\alpha,y_j^\beta)+\mu_2\sum_{\beta=1}^{L}\sum_{\alpha=1}^{N}\omega_\beta\hat{\omega}_\alpha\mathcal{H}_{ij}(x_i^\beta,\hat{y}_j^\alpha)\\&=\sum_{\beta=1}^{L}\sum_{\alpha=2}^{N-1}\omega_\beta\hat{\omega}_\alpha\left(\mu_1\mathcal{H}_{ij}(\hat{x}_i^\alpha,y_j^\beta)+\mu_2\mathcal{H}_{ij}(x_i^\beta,\hat{y}_j^\alpha)\right)\\&\quad+\sum_{\beta=1}^{L}\omega_\beta\hat{\omega}_1\left[\mu_1(\mathbf{U}^+_{i-\frac{1}{2},\beta}+\mathbf{U}^-_{i+\frac{1}{2},\beta})+\mu_2(\mathbf{U}^+_{\beta,j-\frac{1}{2}}+\mathbf{U}^-_{\beta,j+\frac{1}{2}})\right].\end{aligned} \tag{3.26}$$

By the mean value theorem for (3.26), there exist some points (x_i^{1*},y_j^{1*}), (x_i^{2*},y_j^{2*}), (x_i^{3*},y_j^{3*}), (x_i^{4*},y_j^{4*}) in cell (i,j) such that

$$\begin{aligned}&\left(\rho_{ij}(x_i^{1*},y_j^{1*}),m_{ij}(x_i^{2*},y_j^{2*}),n_{ij}(x_i^{3*},y_j^{3*}),E_{ij}(x_i^{4*},y_j^{4*})\right)^T\\&=\sum_{\beta=1}^{L}\sum_{\alpha=2}^{N-1}\omega_\beta\frac{\hat{\omega}_\alpha}{1-\hat{\omega}_1-\hat{\omega}_N}\left(\mu_1\mathcal{H}_{ij}(\hat{x}_i^\alpha,y_j^\beta)+\mu_2\mathcal{H}_{ij}(x_i^\beta,\hat{y}_j^\alpha)\right).\end{aligned} \tag{3.27}$$

Substituting (3.23), (3.24), (3.26) and (3.27) into the first equation of scheme (3.22), we have

$$\begin{aligned}\overline{\mathbf{U}}_{ij}^{n+1}&=(1-\hat{\omega}_1-\hat{\omega}_N)\left(\rho_{ij}(x_i^{1*},y_j^{1*}),m_{ij}(x_i^{2*},y_j^{2*}),n_{ij}(x_i^{3*},y_j^{3*}),E_{ij}(x_i^{4*},y_j^{4*})\right)^T\\&+\sum_{\beta=1}^{L}\frac{\omega_\beta\lambda_1}{2}\left[\beta_{i+\frac{1}{2}}\mathbf{U}^+_{i+\frac{1}{2},\beta}-\mathbf{F}(\mathbf{U}^+_{i+\frac{1}{2},\beta},\mathbf{S}^+_{i+\frac{1}{2},\beta})+\beta_{i-\frac{1}{2}}\mathbf{U}^-_{i-\frac{1}{2},\beta}+\mathbf{F}(\mathbf{U}^-_{i-\frac{1}{2},\beta},\mathbf{S}^-_{i-\frac{1}{2},\beta})\right]\\&+\sum_{\beta=1}^{L}\omega_\beta\mu_1\left[(\widehat{\omega}_N-\frac{\lambda_1}{2\mu_1}\beta_{i+\frac{1}{2}})\left(\mathbf{U}^-_{i+\frac{1}{2},\beta}-\frac{\lambda_1}{2\mu_1}(\widehat{\omega}_1-\frac{\lambda_1}{2\mu_1}\beta_{i+\frac{1}{2}})^{-1}\mathbf{F}(\mathbf{U}^-_{i+\frac{1}{2},\beta},\mathbf{S}^-_{i+\frac{1}{2},\beta})\right)\right]\\&+\sum_{\beta=1}^{L}\omega_\beta\mu_1\left[(\widehat{\omega}_1-\frac{\lambda_1}{2\mu_1}\beta_{i-\frac{1}{2}})\left(\mathbf{U}^+_{i-\frac{1}{2},\beta}+\frac{\lambda_1}{2\mu_1}(\widehat{\omega}_1-\frac{\lambda_1}{2\mu_1}\beta_{i-\frac{1}{2}})^{-1}\mathbf{F}(\mathbf{U}^+_{i-\frac{1}{2},\beta},\mathbf{S}^+_{i-\frac{1}{2},\beta})\right)\right]\\&+\sum_{\beta=1}^{L}\frac{\omega_\beta\lambda_2}{2}\left[\beta_{j+\frac{1}{2}}\mathbf{U}^+_{\beta,j+\frac{1}{2}}-\mathbf{F}(\mathbf{U}^+_{\beta,j+\frac{1}{2}},\mathbf{S}^+_{\beta,j+\frac{1}{2}})+\beta_{j-\frac{1}{2}}\mathbf{U}^-_{\beta,j-\frac{1}{2}}+\mathbf{F}(\mathbf{U}^-_{\beta,j-\frac{1}{2}},\mathbf{S}^-_{\beta,j-\frac{1}{2}})\right]\\&+\sum_{\beta=1}^{L}\omega_\beta\mu_2\left[(\widehat{\omega}_N-\frac{\lambda_2}{2\mu_2}\beta_{j+\frac{1}{2}})\left(\mathbf{U}^-_{\beta,j+\frac{1}{2}}-\frac{\lambda_2}{2\mu_2}(\widehat{\omega}_1-\frac{\lambda_2}{2\mu_2}\beta_{j+\frac{1}{2}})^{-1}\mathbf{F}(\mathbf{U}^-_{\beta,j+\frac{1}{2}},\mathbf{S}^-_{\beta,j+\frac{1}{2}})\right)\right]\\&+\sum_{\beta=1}^{L}\omega_\beta\mu_2\left[(\widehat{\omega}_1-\frac{\lambda_2}{2\mu_2}\beta_{j-\frac{1}{2}})\left(\mathbf{U}^+_{j-\frac{1}{2},\beta}+\frac{\lambda_2}{2\mu_2}(\widehat{\omega}_1-\frac{\lambda_2}{2\mu_2}\beta_{j-\frac{1}{2}})^{-1}\mathbf{F}(\mathbf{U}^+_{\beta,j-\frac{1}{2}},\mathbf{S}^+_{\beta,j-\frac{1}{2}})\right)\right].\end{aligned} \tag{3.28}$$

Starting from (3.22) to (3.28) and following the same line as in the proof of Theorem 1, we can easily prove the following result.

Theorem 2. *For the finite volume HWENO scheme (3.22) with approximation polynomials $\mathcal{H}_{ij}(x,y)=(\rho_{ij}(x,y),m_{ij}(x,y),n_{ij}(x,y),E_{ij}(x,y))^T$. Assume $\overline{\mathbf{U}}_{ij}^n\in G$ for all i, j, if*

$$\begin{aligned}\left(\rho_{ij}(x_i^{1*},y_j^{1*}),m_{ij}(x_i^{2*},y_j^{2*}),n_{ij}(x_i^{3*},y_j^{3*}),E_{ij}(x_i^{4*},y_j^{4*})\right)^T\in G,\\ \mathbf{U}^{\pm}_{\beta,y_{j\pm\frac12}},\mathbf{U}^{\pm}_{x_{i\pm\frac12},\beta},\mathbf{U}^{\pm}_{\beta,y_{j\mp\frac12}},\mathbf{U}^{\pm}_{x_{i\mp\frac12},\beta}\in G,\end{aligned}\tag{3.29}$$

then $\overline{\mathbf{U}}_{ij}^{n+1}\in G$ under the CFL condition

$$\Delta t\left(\frac{1}{\Delta x}+\frac{1}{\Delta y}\right)\max_{i,j}\{\beta_{i+\frac12},\beta_{j+\frac12}\}<\widehat{\omega}=\frac{1}{N(N-1)}.\tag{3.30}$$

To enforce the condition (3.29) in Theorem 2, the following limiter can be used for each cell (i,j).

1. We first modify density by

$$\widehat{\rho}_{ij}(x)=\theta_\rho\left(\rho_{ij}(x)-\bar{\rho}_{ij}\right)+\bar{\rho}_{ij},\quad \theta_\rho=\min\left\{1,\frac{\bar{\rho}_{ij}-\varepsilon}{\bar{\rho}_{ij}-\rho_{min}}\right\},\tag{3.31}$$

where $\theta_\rho\in[0,1]$, $\rho_{min}=\min\left\{\rho^{\pm}_{\beta,j\pm\frac12},\rho^{\pm}_{i\pm\frac12,\beta},\rho^{\pm}_{\beta,j\mp\frac12},\rho^{\pm}_{i\mp\frac12,\beta},\rho_{ij}(x_i^1,y_j^1)\right\}$ and $\epsilon=10^{-13}$, then the modified density is given by

$$\begin{aligned}&\widehat{\rho}^{+}_{\beta,j-\frac12}=\theta_\rho\left(\rho^{+}_{\beta,j-\frac12}-\bar{\rho}^n_{ij}\right)+\bar{\rho}^n_{ij},\quad \widehat{\rho}^{-}_{\beta,j+\frac12}=\theta_\rho\left(\rho^{-}_{\beta,j+\frac12}-\bar{\rho}^n_{ij}\right)+\bar{\rho}^n_{ij},\\ &\widehat{\rho}^{+}_{i-\frac12,\beta}=\theta_\rho\left(\rho^{+}_{i-\frac12,\beta}-\bar{\rho}^n_{ij}\right)+\bar{\rho}^n_{ij},\quad \widehat{\rho}^{-}_{i+\frac12,\beta}=\theta_\rho\left(\rho^{-}_{i+\frac12,\beta}-\bar{\rho}^n_{ij}\right)+\bar{\rho}^n_{ij}.\end{aligned}$$

Let $\widehat{\mathcal{H}}_{ij}(x,y)=\left(\hat{\rho}_{ij}(x,y),m_{ij}(x,y),n_{ij}(x,y),E_{ij}(x,y)\right)^T$. Denote

$$\begin{aligned}&\widehat{q}^1_{ij}=\widehat{\mathcal{H}}_{i+\frac12,j+\frac{\sqrt3}{6}},\quad \widehat{q}^2_{ij}=\widehat{\mathcal{H}}_{i+\frac12,j-\frac{\sqrt3}{6}},\quad \widehat{q}^3_{ij}=\widehat{\mathcal{H}}_{i+\frac{\sqrt3}{6},j-\frac12},\quad \widehat{q}^4_{ij}=\widehat{\mathcal{H}}_{i-\frac{\sqrt3}{6},j-\frac12},\\ &\widehat{q}^5_{ij}=\widehat{\mathcal{H}}_{i-\frac12,j-\frac{\sqrt3}{6}},\quad \widehat{q}^6_{ij}=\widehat{\mathcal{H}}_{i-\frac12,j+\frac{\sqrt3}{6}},\quad \widehat{q}^7_{ij}=\widehat{\mathcal{H}}_{i-\frac{\sqrt3}{6},j+\frac12},\quad \widehat{q}^8_{ij}=\widehat{\mathcal{H}}_{i+\frac{\sqrt3}{6},j+\frac12},\end{aligned}$$

and

$$\begin{aligned}\widehat{q}^9_{ij}&=\left(\widehat{\rho}_{ij}(x_i^{1*},y_j^{1*}),m_{ij}(x_i^{2*},y_j^{2*}),n_{ij}(x_i^{3*},y_j^{3*}),E_{ij}(x_i^{4*},y_j^{4*})\right)^T\\ &=\frac{\overline{\mathbf{U}}^n_{ij}-\sum_{k=1}^L\omega_k\widehat{\omega}_1\left[\frac{\lambda_1}{\mu}(\widehat{\mathcal{H}}^{-}_{i+\frac12,k}+\widehat{\mathcal{H}}^{+}_{i-\frac12,k})+\frac{\lambda_2}{\mu}(\widehat{\mathcal{H}}^{-}_{k,j+\frac12}+\widehat{\mathcal{H}}^{+}_{k,j-\frac12})\right]}{1-2\hat{\omega}_1}.\end{aligned}$$

Define $\overline{\rho e}_{ij}=\overline{E}_{ij}-\frac12\frac{\overline{m}^2_{ij}}{\overline{\rho}_{ij}}-\frac12\frac{\overline{n}^2_{ij}}{\overline{\rho}_{ij}}$ and let $\widehat{\rho e}(\mathbf{U}_{ij}(x,y))=E_{ij}(x,y)-\frac12\frac{m_{ij}(x,y)^2}{\widehat{\rho}_{ij}(x,y)}-\frac12\frac{n_{ij}(x,y)^2}{\widehat{\rho}_{ij}(x,y)}$.

2. To enforce the positivity of internal energy, we modify the internal energy by

$$\widetilde{\mathcal{H}}_{ij}(x,y)=\theta_e\left(\widehat{\mathcal{H}}_{ij}(x,y)-\overline{\mathbf{U}}_{ij}\right)+\overline{\mathbf{U}}_{ij},\quad \theta_e=\min\left\{1,\frac{\overline{\rho e}_{ij}-\varepsilon}{\overline{\rho e}_{ij}-\min\limits_{l=1,\cdots,9}\left\{\widehat{\rho e}(\hat{q}^l_{ij})\right\}}\right\},\tag{3.32}$$

where $\theta_e\in[0,1]$ and $\widehat{\rho e}_{min}=\min\limits_{l=1,\cdots,9}\left\{\widehat{\rho e}(\hat{q}^l_{ij})\right\}$. Actually we only need to obtain the point value $\widetilde{\mathbf{U}}^{\pm}_{i\mp\frac12,\beta}=\widetilde{\mathcal{H}}^{\pm}_{i\mp\frac12,\beta}$, $\widetilde{\mathbf{U}}^{\pm}_{\beta,j\mp\frac12}=\widetilde{\mathcal{H}}^{\pm}_{\beta,j\mp\frac12}$, we define the internal energy function as $\Psi(\mathbf{U})=E-\frac12\frac{m^2}{\rho}-\frac12\frac{n^2}{\rho}$. For $l=1,\cdots,9$, if $\Psi\left(\widehat{\rho e}(\hat{q}^l_{ij})\right)<\varepsilon$, then set $t^l_\varepsilon=\frac{\Psi(\overline{\mathbf{U}}_{ij})-\varepsilon}{\Psi(\overline{\mathbf{U}}_{ij})-\Psi\left(\widehat{\rho e}(\hat{q}^l_{ij})\right)}$; if $\Psi\left(\widehat{\rho e}(\hat{q}^l_{ij})\right)\geq\varepsilon$, then set $t^l_\varepsilon=1$. Take $\theta_e=\min\{t^1_\varepsilon,\cdots,t^9_\varepsilon\}$, then

$$\widetilde{\mathbf{U}}^{-}_{i+\frac{1}{2},\beta} = \widetilde{\mathcal{H}}^{-}_{i+\frac{1}{2},\beta} = \theta_e\left(\widehat{\mathcal{H}}^{-}_{i+\frac{1}{2},\beta} - \overline{\mathbf{U}}_{ij}\right) + \overline{\mathbf{U}}_{ij},$$

$$\widetilde{\mathbf{U}}^{+}_{i-\frac{1}{2},\beta} = \widetilde{\mathcal{H}}^{+}_{i-\frac{1}{2},\beta} = \theta_e\left(\widehat{\mathcal{H}}^{+}_{j-\frac{1}{2},\beta} - \overline{\mathbf{U}}_{ij}\right) + \overline{\mathbf{U}}_{ij},$$

$$\widetilde{\mathbf{U}}^{-}_{\beta,j+\frac{1}{2}} = \widetilde{\mathcal{H}}^{-}_{\beta,j+\frac{1}{2}} = \theta_e\left(\widehat{\mathcal{H}}^{-}_{\beta,j+\frac{1}{2}} - \overline{\mathbf{U}}_{ij}\right) + \overline{\mathbf{U}}_{ij},$$

$$\widetilde{\mathbf{U}}^{+}_{\beta,j-\frac{1}{2}} = \widetilde{\mathcal{H}}^{+}_{\beta,j-\frac{1}{2}} = \theta_e\left(\widehat{\mathcal{H}}^{+}_{\beta,j-\frac{1}{2}} - \overline{\mathbf{U}}_{ij}\right) + \overline{\mathbf{U}}_{ij}.$$

Finally, use $\widetilde{\mathbf{U}}^{\pm}_{i\mp\frac{1}{2},\beta}, \widetilde{\mathbf{U}}^{\pm}_{\beta,j\mp\frac{1}{2}}$ instead of $\mathbf{U}^{\pm}_{i\mp\frac{1}{2},\beta}, \mathbf{U}^{\pm}_{\beta,j\mp\frac{1}{2}}$ in the scheme (3.22).

Remark 3.3. Notice that we mainly introduce the design and implementation of positivity-preserving property of two-dimensional FV hybrid HWENO scheme. $\overline{\mathbf{U}}^n_{ij}, \overline{\mathbf{V}}^n_{ij}$ and $\overline{\mathbf{W}}^n_{ij}$ in (3.21) are applied to HWENO interpolation for the approximation of the function $\mathbf{U}$ and its partial derivative $\mathbf{S}$ in Gauss-Labotto points, and the detailed procedures of FV hybrid HWENO interpolation in two dimensional case are given in the appendix A.

Remark 3.4. Similar to the one-dimensional case, the approximation polynomials are not needed for implementing the limiter (3.31) and (3.32). And it is a high order accurate and conservative limiter, see [26].

3.3. Implementation of CFL constraints

In this paper, we use (2.6) for high order time discretization. Since strong stability preserving (SSP) Runge-Kutta time discretization is a convex combination of forward Euler steps and G is convex, Theorem 1 and Theorem 2 still hold for (2.6) if the CFL is one third of (3.12) and (3.30). However, the CFL constraints (3.12) and (3.30) should not be used directly for at least two reasons. First, since $|u| + \frac{1}{2\rho^2 e}(\sqrt{\rho^2 q^2 + 2\rho^2 e|\tau - p|^2} + \rho|q|) = O(1)$ for a smooth solution, the CFL constraints (3.12) and (3.30) give $\Delta t = \mathcal{O}(\Delta x)$ which do not necessarily satisfy the linear stability constraints $\Delta t = \mathcal{O}(\mathrm{Re}\Delta x^2)$ for any explicit time discretizations. In other words, the time step should also satisfy $\Delta t = \mathcal{O}(\mathrm{Re}\Delta x^2)$ besides (3.12) and (3.30). Second, the time step constraints (3.12) and (3.30) is a sufficient condition but may not be a necessary condition for $\overline{\mathcal{U}}^{n+1}_K \in G$, thus in practice it should not be used directly for the sake of efficiency.

To this end, we can use the same simple time marching strategy in [26]. The positivity preserving limiter should be used for each stage in (2.6) and we can implement the positivity-preserving high order finite volume hybrid HWENO scheme with the third order SSP Runge-Kutta (2.6) for equation (2.1) as follows:

Step 1. At time level n, for the given $\overline{\mathcal{U}}^n_K \in G$. Compute the wave speed $\alpha_i = |u_i| + \sqrt{\frac{\gamma p_i}{\rho_i}}$. Let $\alpha^\star = \max_i |\alpha_i|$ taken over all edges, $\Delta x = \min_K \frac{|K|}{|e_K|}$ and e_K is the longest edge in cell K set the time step

$$\Delta t = \min\left\{a\frac{1}{\alpha^\star}\Delta x, b\mathrm{Re}\Delta x^2\right\}, \tag{3.33}$$

where the two parameters are set as $a = \frac{1}{12}$ and $b = 0.001$ for compressible Navies-Stokes equations. For compressible Euler equations, it is replaced by $\Delta t = \frac{1}{12\alpha^\star}\Delta x$ since $\mathrm{Re} = \infty$.

Step2. Compute the first stage, denoted by $\overline{\mathcal{U}}^{(1)}_K$. If the cell average $\overline{\mathcal{U}}^{(1)}_K \in G$, then proceed to next step. Otherwise $\overline{\mathcal{U}}^{(1)}_K$ has negative density or pressure, then recompute the first stage with a time step halved.

Step3. For the given $\overline{\mathcal{U}}^{(1)}_K \in G$, compute the second stage, denoted by $\overline{\mathcal{U}}^{(2)}_K$. If the cell average $\overline{\mathcal{U}}^{(2)}_K \in G$, then proceed to next step. Otherwise $\overline{\mathcal{U}}^{(2)}_K$ has negative density or pressure, then return the Step2 and restart the computation with a time step halved.

Step4. For the given $\overline{\mathcal{U}}^{(2)}_K \in G$, compute the $\overline{\mathcal{U}}^{(n+1)}_K$. If the cell average $\overline{\mathcal{U}}^{(n+1)}_K \in G$, then the computation to time step $n+1$ is done. Otherwise $\overline{\mathcal{U}}^{(n+1)}_K$ has negative density or pressure, then return the Step2 and restart the computation with a time step halved.

Theorem 1 and Theorem 2 imply that the implementation above will not result in any infinite loops and the restarting is ensured to stop when time step constraints (3.12) and (3.30) are met for each stage.

4. Numerical tests

In this section, we test the positivity-preserving (PP) high order finite volume hybrid HWENO scheme with the third order SSP Runge-Kutta method on several demanding examples. For HWENO reconstruction, quintic polynomial reconstruction is used in one dimension, and cubic polynomial reconstruction is used in two dimensions. The hybrid HWENO scheme

Table 4.1
Accuracy test of the PP hybrid HWENO scheme for one-dimensional and two-dimensional compressible Navier-Stokes equations with Re = 100, the L_1 and L_∞ errors are showed.

Mesh	L_∞ Error	L_∞ Order	L_1 Error	L_1 Order
20	1.21 E-2	–	5.90 E-3	–
40	2.23 E-3	2.44	6.65 E-4	3.15
80	5.58 E-5	5.32	1.44 E-5	5.53
160	1.10 E-6	5.66	2.46 E-7	5.87
320	2.25 E-8	5.61	7.13 E-9	5.11
640	6.35 E-10	5.15	2.14 E-10	5.06
10×10	$1.08E$-3	–	$2.25E$-4	–
20×20	$1.32E$-4	3.04	$1.73E$-5	3.70
40×40	$1.05E$-5	3.65	$1.24E$-6	3.80
80×80	$6.07E$-7	4.11	$7.71E$-8	4.01
160×160	$2.93E$-8	4.37	$4.53E$-9	4.09
320×320	$1.54E$-9	4.25	$2.70E$-10	4.07

in [32] will blow up for Examples 4.3-4.7 for compressible Euler equations due to loss of positivity. The same positivity-preserving methods in Section 3 also apply to the HWENO scheme without any hybridization, which is also tested. The CPU time of the PP hybrid FV HWENO scheme and the PP FV HWENO scheme is listed in Table 4.2. The only difference in these two schemes is in the reconstruction step: the HWENO scheme uses nonlinear HWENO reconstruction in all cells, whereas the hybrid HWENO scheme uses the nonlinear HWENO reconstruction only in troubled cells and uses linear reconstruction in other cells, e.g., smooth regions. Moreover, on troubled cells, the hybrid HWENO scheme uses one more non-oscillatory limiter on the first-order moment variables, as a preprocessing step before the HWENO reconstruction, see [32] for details of the troubled cell indicator and the non-oscillatory limiter on the first-order moment.

Example 4.1. Accuracy test. We test the accuracy of the PP hybrid HWENO scheme for compressible Navier-Stokes equations in one and two dimensions with Re = 100. For one-dimensional equation (3.1), the initial condition is $\rho = 1,\ u = 0,\ E = \frac{12}{\gamma-1} + \frac{1}{2}\exp(-4(\cos(x/2))^2)$ on the interval $[0, 2\pi]$. For two-dimensional equation (3.16), the initial condition is $\rho = 1, u = v = 0, E = \frac{12}{\gamma-1} + \frac{1}{2}\exp(-4(\cos(x/2))^2 - 4(\cos(y/2))^2)$ on the rectangle domain $[0, 2\pi] \times [0, 2\pi]$. The boundary condition is periodic. The reference solution was generated by a Fourier collocation spectral method using 1280 points and a 1280×1280 mesh in one and two dimensions respectively. The reconstruction polynomial has degree four in one dimension and, degree three in two dimensions. The errors in Table 4.1 verify the accuracy of the diffusion flux and the limiter.

We can see that the PP hybrid HWENO scheme achieves fifth order accuracy in one dimension and fourth order accuracy in two dimensions, which is consistent with the designed order of accuracy of the HWENO scheme.

Example 4.2. The Lax problem. The initial condition is

$$(\rho, u, p, \gamma) = \begin{cases} (0.445, 0.698, 3.528, 1.4), & x \in [0, 5) \\ (0.5, 0, 0.571, 1.4), & x \in [0, 5]. \end{cases} \tag{4.1}$$

The final computing time is $T = 1.3$. See [26] for how the reference solution can be generated. See Fig. 4.1 for results of the HWENO scheme without hybridization of linear reconstruction and the positivity-preserving limiter. Even though the HWENO scheme produces non-oscillatory solutions for Re = 100 in Fig. 4.1, oscillations will emerge and stability will be lost for larger Reynolds number. The oscillations can be observed for the numerical solutions of compressible Euler equations, namely Re = ∞ in Fig. 4.1. This indicates that, for the HWNEO scheme based on the reconstruction of the zero-order and first-order moment without modifying the first order moment in troubled cell, itself is unstable.

See Fig. 4.2 for the results of the PP hybrid HWENO scheme, which produces non-oscillatory solutions with a good resolution. About 2.43% and 2.68% cells are troubled cells for Re = 1000 and ∞ respectively. For other cells, a linear approximation is used thus the PP hybrid HWENO scheme saves about 77.68% and 75.08% computational time compared to the PP HWENO scheme as shown in Table 4.2. Notice that PP limiter was not triggered in the PP hybrid HWENO scheme in this test as shown in Table 4.2, which is due to the additional non-oscillatory limiter on the first-order moment in troubled cells. In other words, the hybrid HWENO scheme without any PP limiter is already very stable, for the Lax problem. In addition, there is a little dent in the plot of the velocity (the left figure of the second row of Fig. 4.2). This is indeed a numerical artifact in PP hybrid HWENO scheme. For example, the numerical solution velocity of the FV WENO scheme in [13] showed a similar dent.

From the bottom row of Fig. 4.2, we observe that there are less troubled cells for the case Re = 1000 thus the non-oscillatory first-order moment limiter is used on less cells, compared to the case Re = ∞. Roughly speaking, the non-oscillatory first-order moment limiter simply induces artificial viscosity. For this reason, the numerical results of PP hybrid HWENO scheme for Re = 1000 have slightly better resolution at the discontinuity than the numerical results of PP hybrid HWENO scheme for Re = ∞. This phenomenon is also observed in other numerical tests.

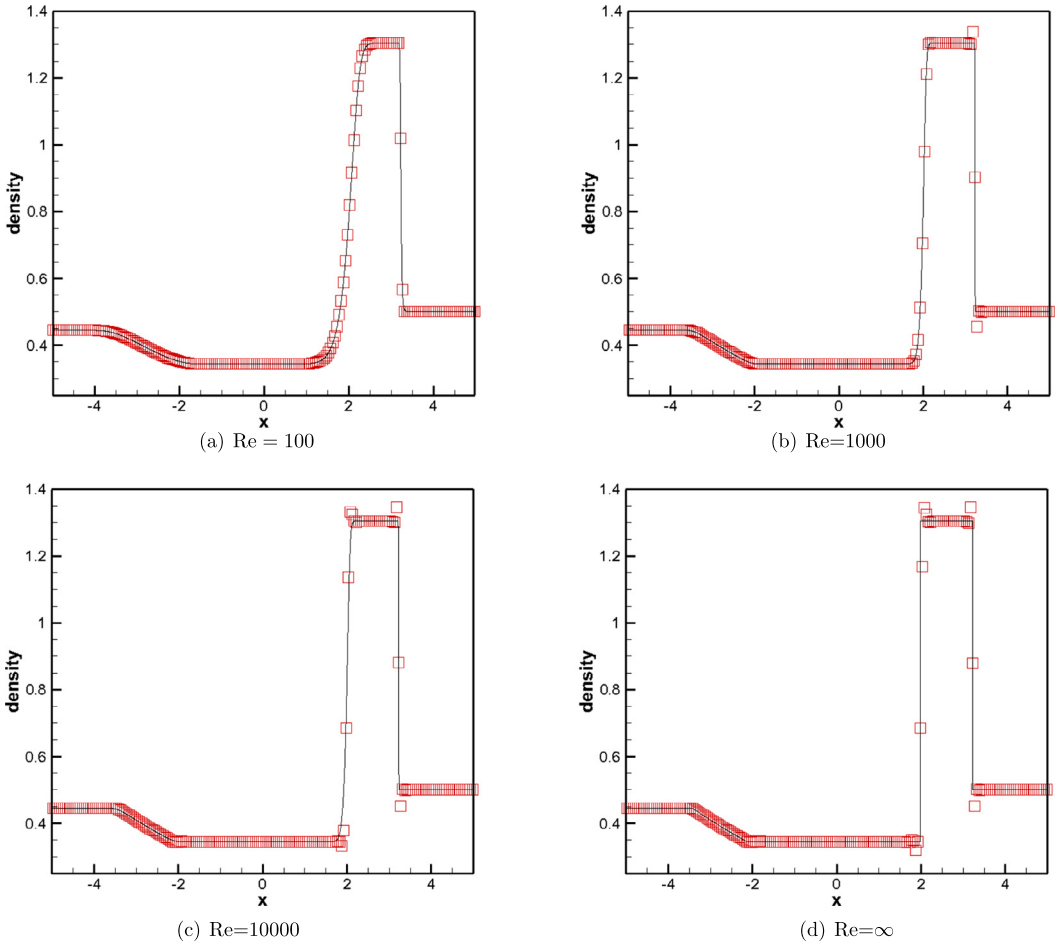

Fig. 4.1. The Lax shock tube problem. $T = 1.3$. Solid line: the reference solution; squares: the results of the HWENO scheme on uniform 200 cells. (For interpretation of the colors in the figure(s), the reader is referred to the web version of this article.)

Table 4.2
CPU time: the total computing time in seconds for the PP hybrid HWENO scheme and the PP HWENO scheme to solve compressible NS equations; Time saving ratios: the CPU time saving ratios of the total CPU time by the PP hybrid HWENO scheme over the PP HWENO scheme on the same numerical example; PP limiter ratio: the ratio of PP limiter triggered (either $\theta_\rho < 1$ or $\theta_e < 1$) cells over the total cells.

Numerical example	PP hybrid HWENO scheme		PP HWENO scheme		Time saving ratios
	CPU time	PP limiter	CPU time	PP limiter	
$Re = \infty$					
4.2 1D Lax problem	2.45	0.00%	8.16	0.00%	69.98%
4.3 Double rarefraction problem	1.63	10.00%	3.98	10.00%	59.05%
4.4 1D Sedov problem	17.61	3.00%	56.55	3.00%	68.86%
4.5 Leblanc problem	71.77	0.25%	628.86	0.25%	88.59%
4.6 2D Sedov problem	9611.84	1.09%	25726.30	1.09%	62.64%
4.7 Shock-diffraction problem	13776.48	0.23%	38014.60	0.23%	63.76%
$Re = 1000$					
4.2 1D Lax problem	2.20	0.00%	7.64	0.00%	71.20%
4.3 Double rarefraction problem	9.88	10.00%	30.25	10.00%	67.34%
4.4 1D Sedov problem	21.56	3.00%	69.59	3.00%	69.02%
4.5 Leblanc problem	96.97	0.25%	935.99	0.25%	89.64%
4.6 2D Sedov problem	11764.44	1.09%	32355.45	1.09%	63.64%
4.7 Shock-diffraction problem	17183.64	0.23%	48318.10	0.23%	64.45%

Example 4.3. The 1D double rarefaction problem. This test case has the low pressure and low density region. Negative density or pressure can be easily produced in many high order numerical schemes, resulting in blow up of the computation. The initial condition is

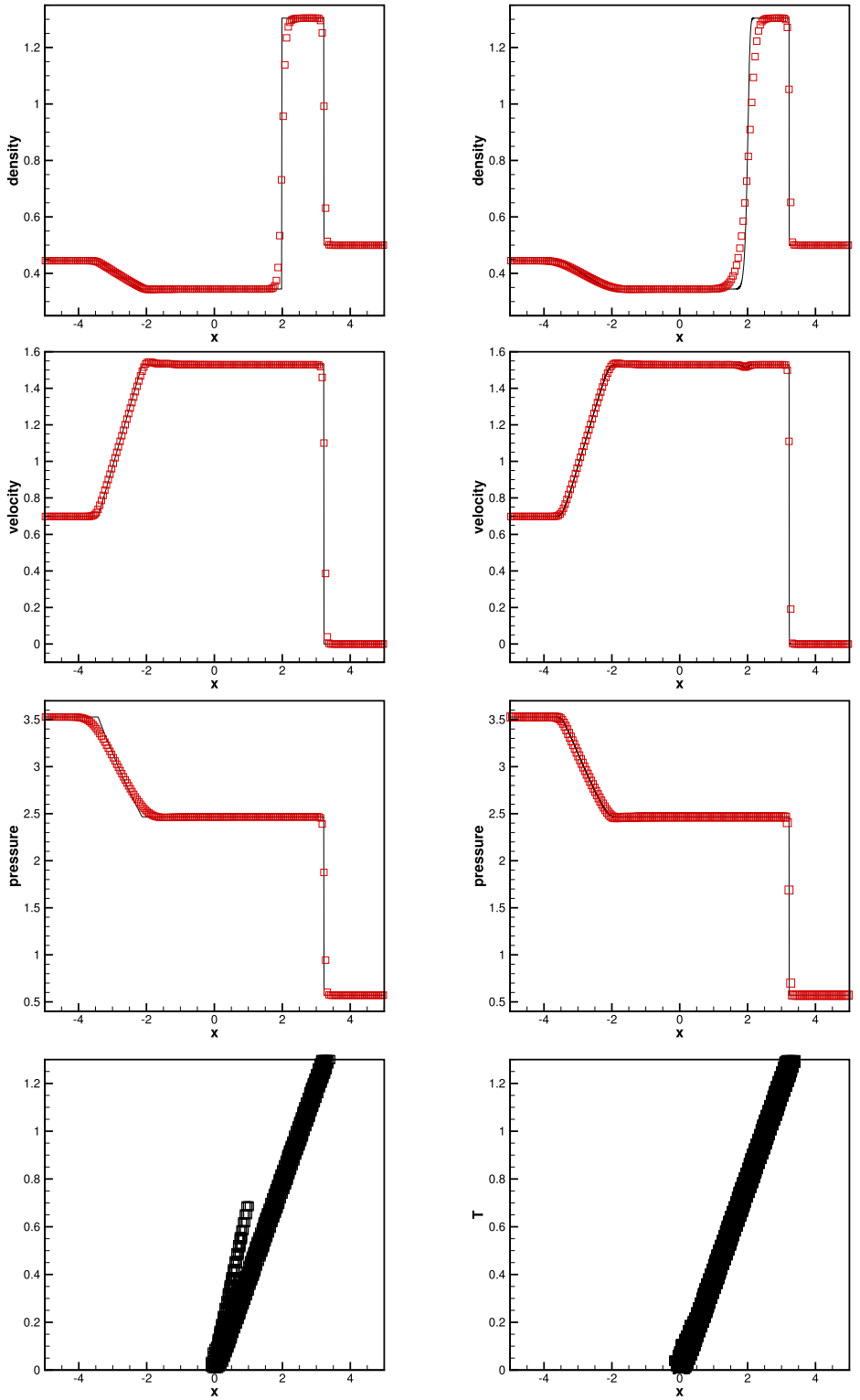

Fig. 4.2. The Lax problem. T = 1.3 for Re = ∞ (Left) and 1000 (Right). From top to bottom: density, velocity, pressure, time history of troubled cells in the PP hybrid HWENO scheme. Solid line: the reference solution; squares: PP hybrid HWENO scheme on uniform 200 cells.

$$(\rho, u, p, \gamma) = \begin{cases} (7, -1, 0.2, 1.4), & x \in [-1, 0), \\ (7, 1, 0.2, 1.4), & x \in [0, 1]. \end{cases} \tag{4.2}$$

The final computing time is T = 0.6. The left and right boundary conditions are inflow and outflow respectively. The numerical results of PP hybrid HWENO scheme are shown in Fig. 4.3 for Re = 1000 and ∞. About 11.30% and 19.57% cells are troubled cells for Re = 1000 and Re = ∞. The PP hybrid HWENO scheme saves 67.34% and 59.05% CPU time compared to the PP HWENO scheme respectively.

Example 4.4. The 1D Sedov problem. This test involves both very low density and strong shocks. The exact solution for Euler equation is specified in [9,21]. The computational domain is $[-2, 2]$ and initial conditions are that the density is 1, the velocity is 0, the total energy is 10^{-12} everywhere except in the center cell, which is a constant $E_0/\Delta x$ with $E_0 = 3200000$, with $\gamma = 1.4$. The inlet and outlet conditions are imposed on the left and right boundaries, respectively. The final compute time is T = 0.001 and computational results of the PP hybrid HWENO scheme are presented in Fig. 4.4. About 14.50% cells are troubled cells, and 68.86% CPU time is saved compared to HWENO scheme for compressible Euler equations. For compressible Navier-Stokes equations, there are 11.92% troubled cells, and 69.02% CPU time is saved compared to the PP HWENO scheme.

Example 4.5. The Leblanc problem. The initial condition is

$$(\rho, u, p, \gamma) = \begin{cases} (2, 0, 10^9, 1.4), & x \in [-10, 0), \\ (0.001, 0, 1, 1.4), & x \in [0, 10]. \end{cases} \tag{4.3}$$

The inlet and outlet conditions are imposed on the left and right boundaries, respectively. The computational results of the PP hybrid HWENO scheme at the final time $T = 0.0001$ are presented in Fig. 4.5. About 0.97% and 1.35% cells are troubled cells for Re = 1000 and ∞ respectively, and about 89.64% and 88.59% computational time is saved compared to the PP HWENO scheme.

Example 4.6. The 2D Sedov problem. The computational domain is a square of $[0, 1.1] \times [0, 1.1]$. For the initial condition, similar to the 1D case, the density is 1, the velocity is 0, the total energy is 10^{-12} everywhere except in the lower left corner is the constant $\frac{0.244816}{\Delta x \Delta y}$ and $\gamma = 1.4$. The numerical boundary on the left and bottom edges is reflective. The numerical boundary on the right and top is outflow. The results at the final time T = 1 of the PP hybrid HWENO schemes are shown in the Fig. 4.6. About 13.82% and 14.62% cells are troubled cells for Re = 1000 and ∞, and 63.64% and 62.64% computational time is saved compared to the PP HWENO scheme.

Example 4.7. The shock diffraction problem. The computational domain is the union of $[0, 1] \times [6, 11]$ and $[1, 13] \times [0, 11]$. The initial condition is a pure right-moving shock of Mach number 5.09, initially located at $x = 0.5$ and $6 \le y \le 11$, moving into undisturbed air ahead of the shock with a density of 1.4 and a pressure of 1. The boundary conditions are inflow at $x = 0, 6 \le y \le 11$, outflow at $x = 13, 0 \le y \le 11, 1 \le x \le 13, y = 0$ and $0 \le x \le 13, y = 11$, and reflective at the walls $0 \le x \le 1, y = 6$ and at $x = 1, 0 \le y \le 6$. The final computing time T = 2.3. It is well known that the diffraction of high speed shock waves at sharp angles leads to low density and low pressure. See Fig. 4.7 for the results. For compressible Euler equations, about 5.07% cells are troubled cells, and 63.76% CPU time is saved compared to the PP HWENO scheme. For compressible Navier-Stokes equations, about 4.39% cells are troubled cells, and 64.45% CPU time is saved compared to the PP HWENO scheme.

5. Concluding remarks

In this paper, we have constructed the positivity-preserving FV hybrid HWENO scheme for solving compressible NS equations, based on the work in [26,32]. For compressible Euler equations, the scheme is much more robust than hybrid HWENO schemes in [32]. For both Euler and Navier-Stokes equations, it performs well on representative challenging low density and low pressure problems. Thanks to hybridization techniques, it is not only more efficient than conventional HWENO schemes, but also produces better resolution for high Reynolds number flows due to less artificial viscosity. Numerical tests have demonstrated the robustness and the efficiency of the scheme. Future work includes the extension of the positivity-preserving FV hybrid HWENO scheme to unstructured meshes and the positivity-preserving finite difference WENO scheme for compressible Navier-Stokes equations.

CRediT authorship contribution statement

Chuan Fan: Methodology, Software, Writing – original draft. **Xiangxiong Zhang:** Conceptualization, Methodology, Writing – review & editing. **Jianxian Qiu:** Conceptualization, Methodology, Supervision, Writing – review & editing.

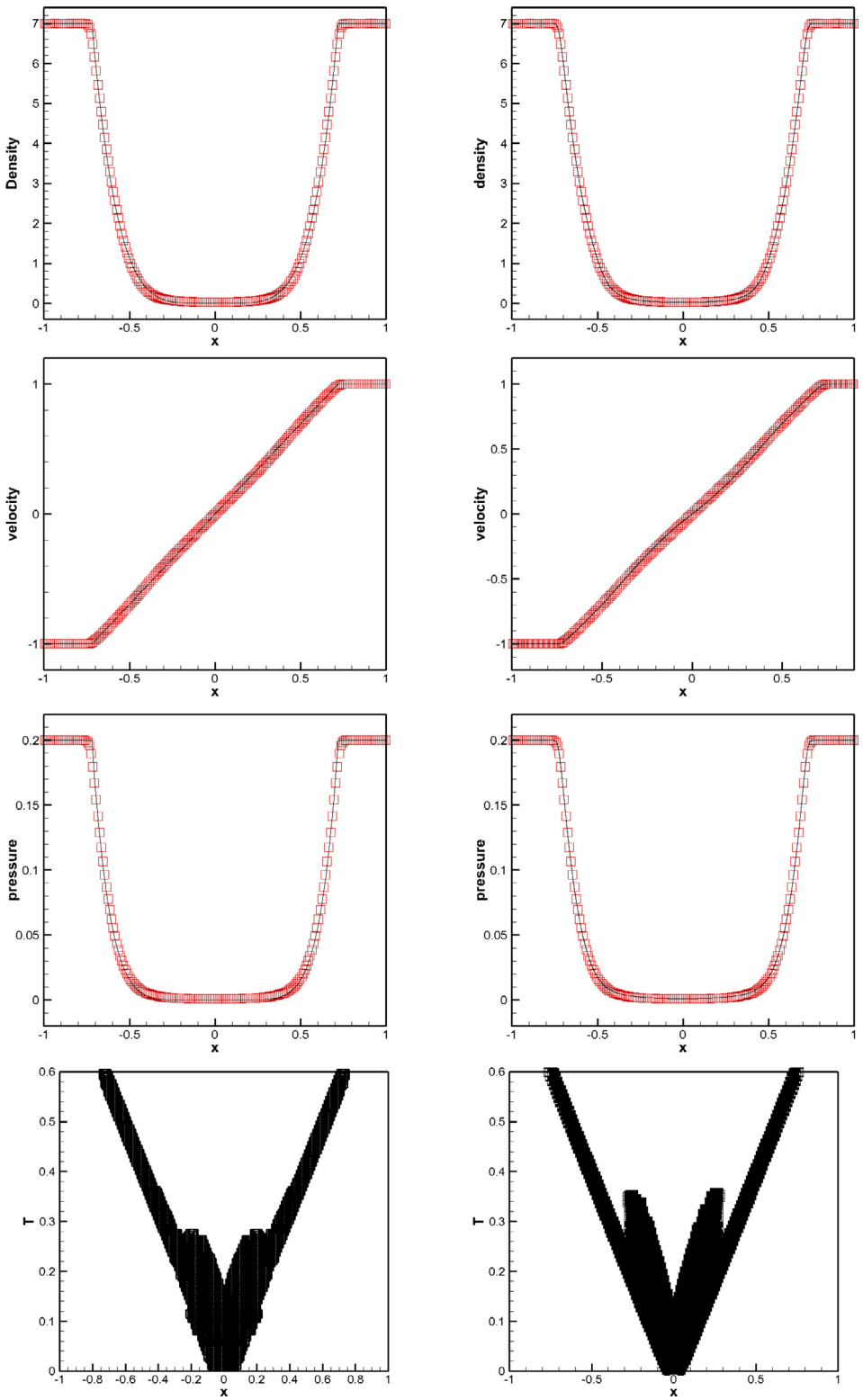

(a) Re=1000 (b) Re=∞

Fig. 4.3. The Double Rarefaction problem. T = 0.6. From top to bottom: density, velocity, pressure, and time history of troubled cells. Re = ∞ (right) and 1000 (left). Solid line: the exact solution; squares: PP hybrid HWENO scheme on uniform 200 cells.

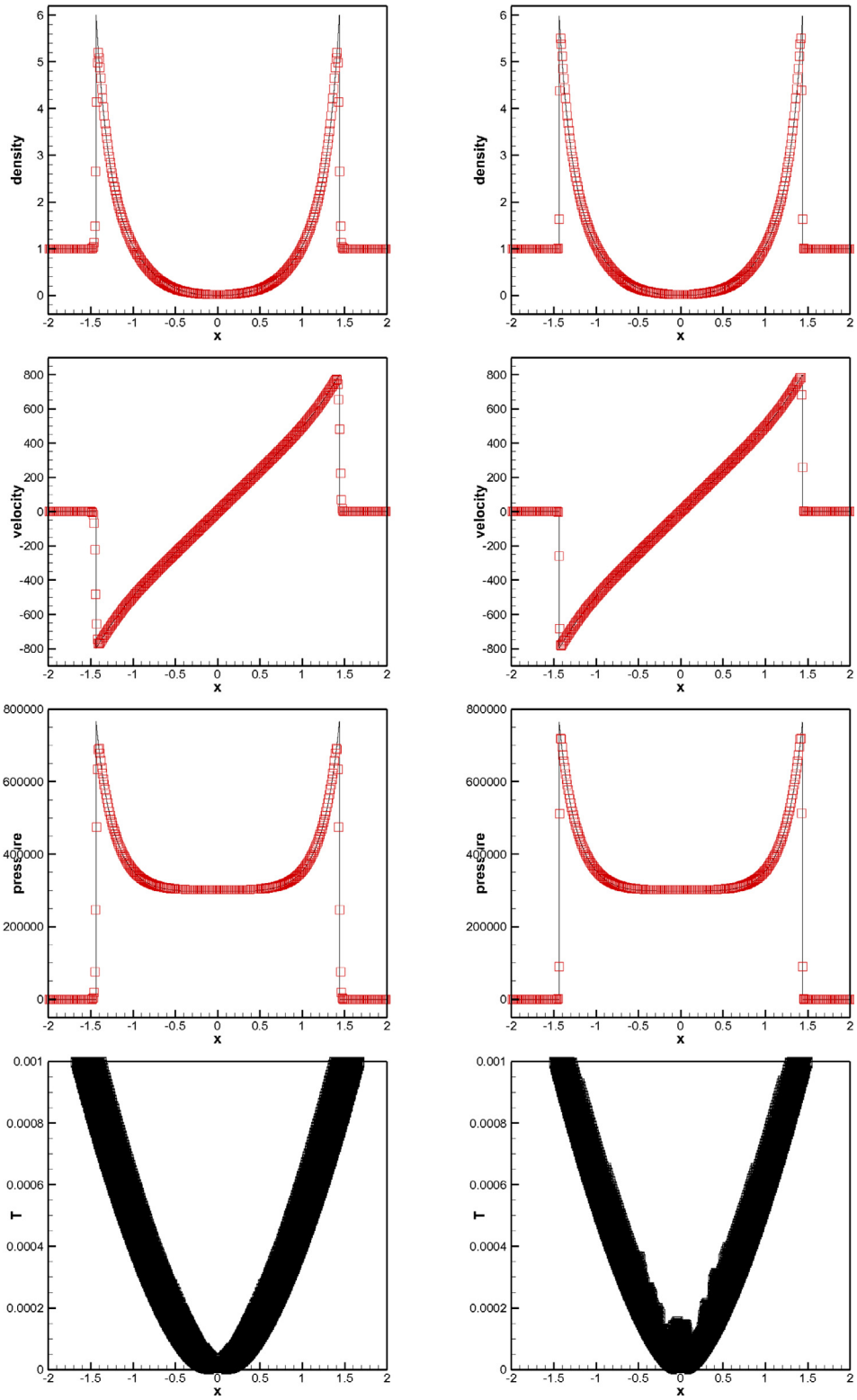

(a) Re=∞ (b) Re=1000

Fig. 4.4. The 1D Sedov problem. $T = 0.001$. From top to bottom: density, velocity, pressure, and time history of troubled cells. $Re = \infty$ (left) and 1000 (right). Solid line: the reference solution; squares: PP hybrid HWENO scheme on uniform 400 cells.

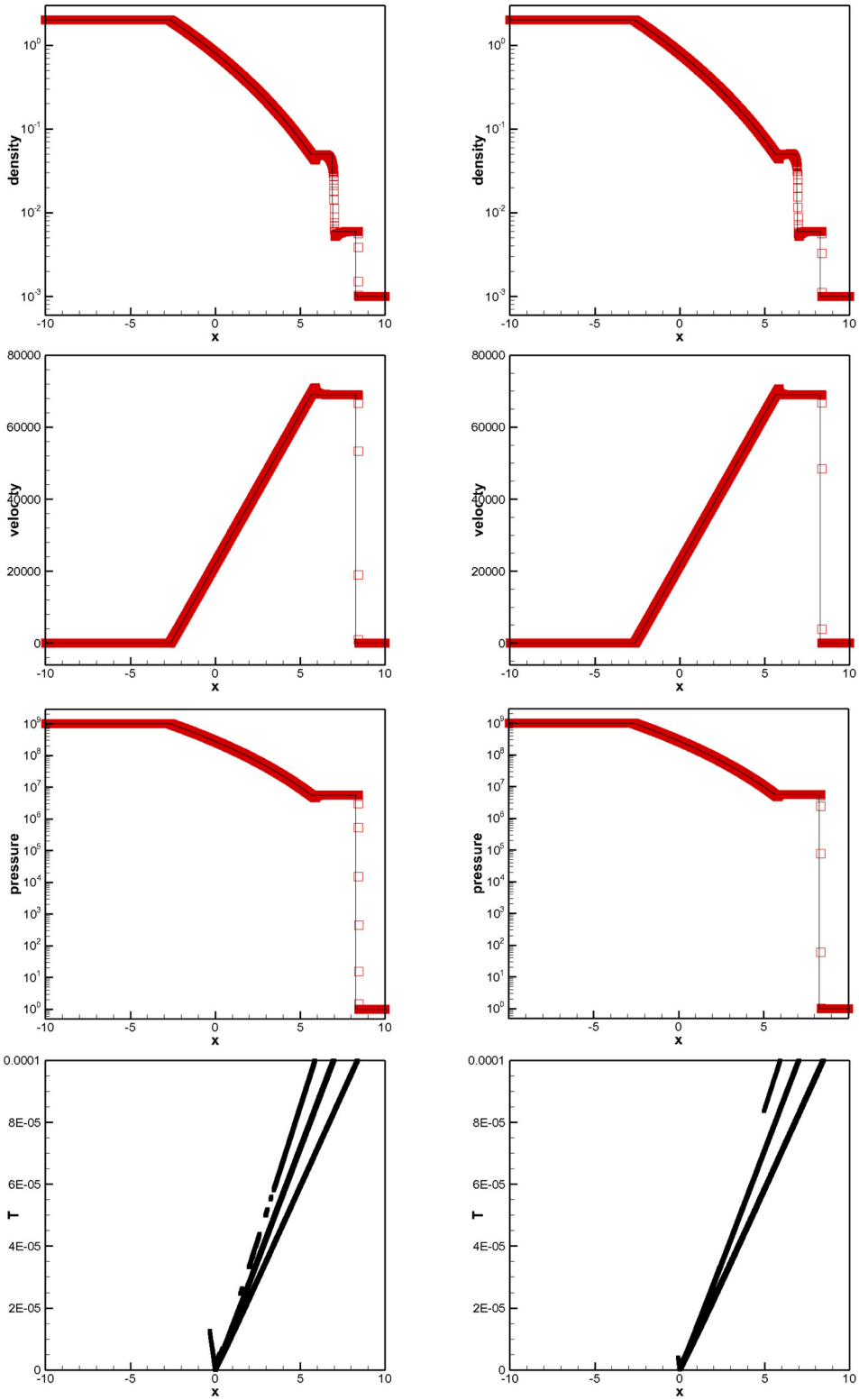

Fig. 4.5. The Leblanc problem. $T = 0.0001$ for $Re = \infty$ (Left) and 1000 (Right). From top to bottom: log plot of density, velocity, log plot of pressure, time history of troubled cells. Solid line: the reference solution; squares: PP hybrid HWENO scheme on uniform 3200 cells.

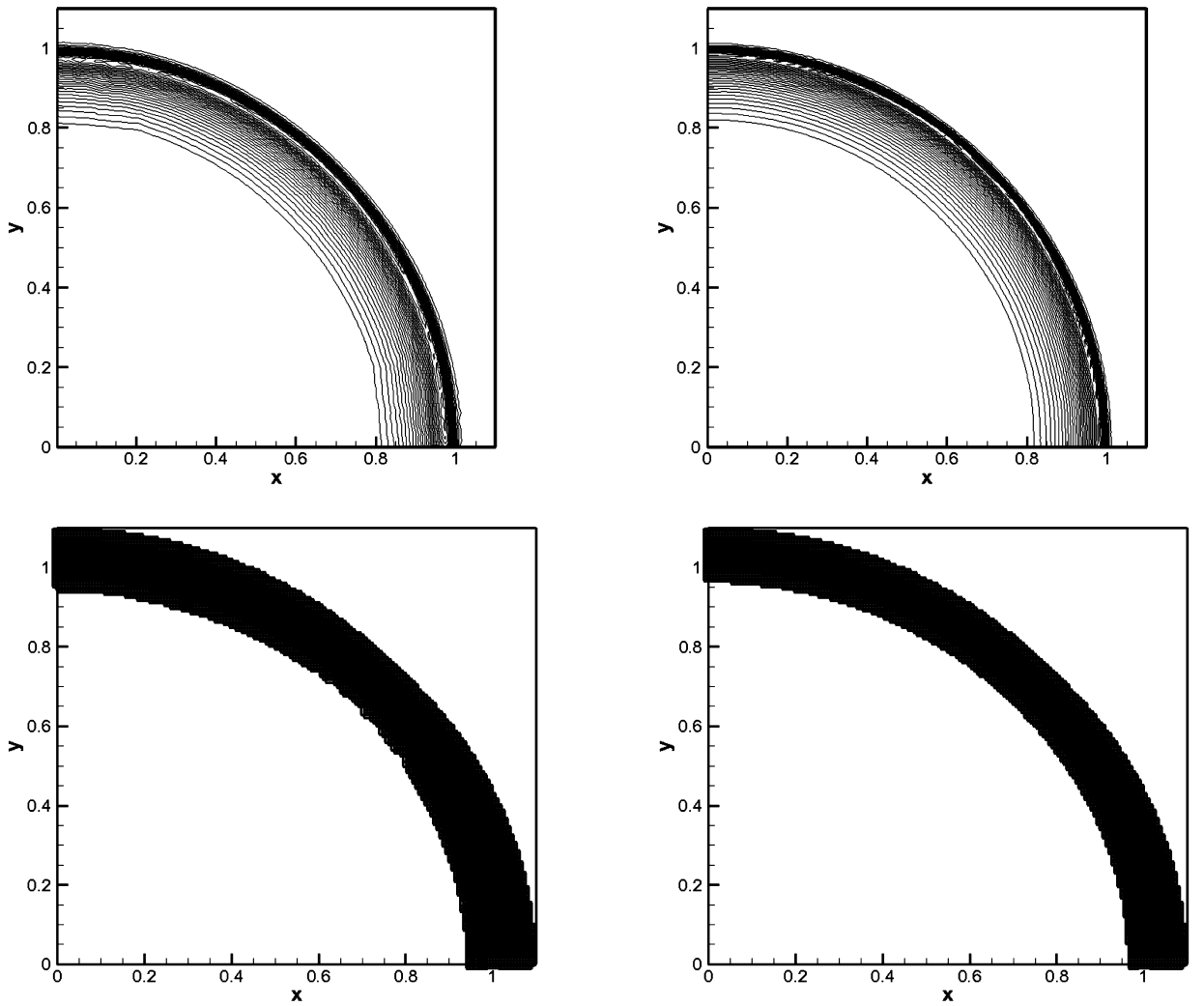

Fig. 4.6. The 2D Sedov problem. $T = 1.0$ for $\mathrm{Re} = \infty$ (Left) and 1000 (Right). Top row: 30 equally spaced contour lines from 0.95 to 5 for density. Bottom row: troubled cells at final time. The PP hybrid HWENO scheme with mesh size $\Delta x = \Delta y = 1.1/160$.

Declaration of competing interest

The authors declare that they have no known competing financial interests or personal relationships that could have appeared to influence the work reported in this paper.

Appendix A

The hybrid HWENO reconstruction for function values $u(x, y)$ at the specific points based on the zeros-order and first-order moment can be found in [32]. To implement the scheme in this paper, we still need a reconstruction of gradients $\nabla u(x, y)$. Here we describe the hybrid HWENO reconstruction for derivative $u_x(x)$ and the partial derivatives $u_x(x, y)$ and $u_y(x, y)$.

A.1. One-dimensional case

We consider the reconstruction procedure for derivative values $(u_x)^{\mp}_{i\pm\frac{1}{2}}$ and $(u_x)_{i\pm\sqrt{5}/10}$ from $\{\overline{u}_i, \overline{v}_i\}$. Here $\overline{u}_i(t) = \frac{1}{\Delta x}\int_{I_i} u(x,t)dx$ is the zeroth order moment and $\overline{v}_i(t) = \frac{1}{\Delta x}\int_{I_i} u(x,t)\frac{x-x_i}{\Delta x}dx$ is the first order moment in I_i. Given the stencils S_1, S_2, S_3 and S_0, similar to hybrid HWENO reconstruction of $(u)^{\mp}_{i\pm\frac{1}{2}}$ and $(u)_{i\pm\sqrt{5}/10}$ in [32], first identify the troubled cell and modify the first order moment in the troubled cell as in [32]. If one of the cells in stencil S_0 is identified as a troubled cell, then apply the HWENO method described in Step A.1 to reconstruct $(u_x)^{\mp}_{i\pm\frac{1}{2}}$; otherwise we use the linear re-

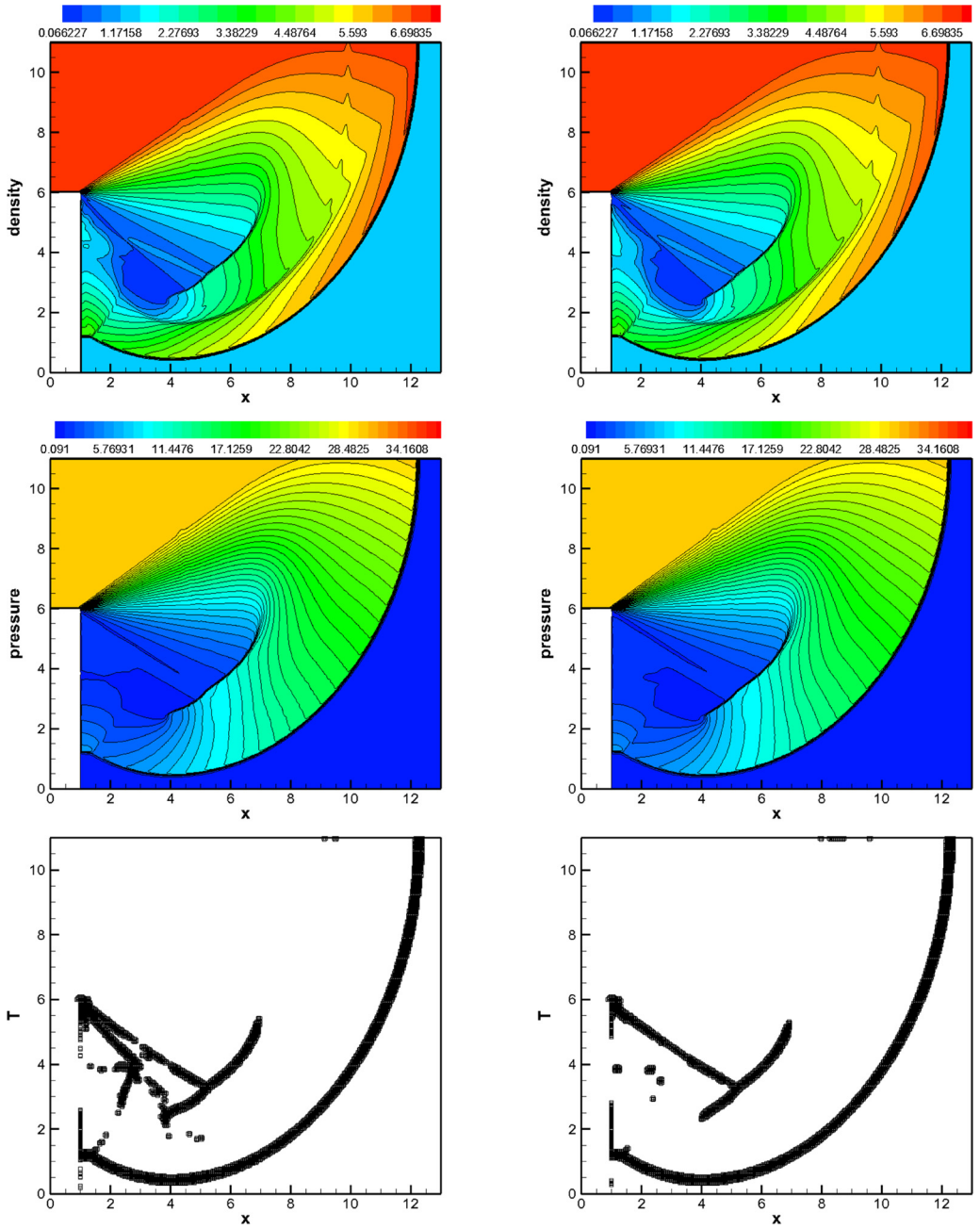

Fig. 4.7. The Shock Diffraction problem. T = 2.3 for Re = ∞(Left) and 1000 (Right). From top to bottom: density 20 equally spaced contour lines from 0.066227 to 7.0668, pressure 40 equally spaced contour lines from 0.091 to 37, and the troubled cells at the final time. The PP hybrid HWENO scheme with mesh size $\Delta x = \Delta y = 1/32$.

construction method described in Step A.2 to reconstruct $(u_x)^{\mp}_{i\pm\frac{1}{2}}$. We use linear reconstruction for $(u_x)_{i\pm\sqrt{5}/10}$ on all cells, as described in Step A.3.

StepA.1. The HWENO reconstruction of $(u_x)^{\mp}_{i\pm\frac{1}{2}}$.

In [32], the reconstruction procedure involves the Hermite cubic polynomials $p_1(x)$, $p_2(x)$, $p_3(x)$ in the small stencils S_1, S_2, S_3 and a Hermite quintic polynomial $p_0(x)$ in a large stencil S_0. Now, we need the derivative of these polynomial at cell boundary $x_{i+\frac{1}{2}}$ in terms of the averages, which can be written as:

$$p_0'(x_{i+\frac{1}{2}}) = \frac{5}{36\Delta x}\bar{u}_{i-1} - \frac{9}{4\Delta x}\bar{u}_i + \frac{19}{9\Delta x}\bar{u}_{i+1} + \frac{11}{18\Delta x}\bar{v}_{i-1} - \frac{97}{18\Delta x}\bar{v}_i - \frac{62}{9\Delta x}\bar{v}_{i+1}.$$

$$
\begin{aligned}
p_1'(x_{i+\frac{1}{2}}) &= \frac{21}{4\Delta x}\bar{u}_{i-1} - \frac{21}{4\Delta x}\bar{u}_i + \frac{51}{2\Delta x}\bar{v}_{i-1} + \frac{99}{2\Delta x}\bar{v}_i,\\
p_2'(x_{i+\frac{1}{2}}) &= \frac{5}{22\Delta x}\bar{u}_{i-1} - \frac{1}{\Delta x}\bar{u}_i + \frac{17}{22\Delta x}\bar{u}_{i+1} + \frac{60}{11\Delta x}\bar{v}_i,\\
p_3'(x_{i+\frac{1}{2}}) &= -\frac{9}{4\Delta x}\bar{u}_i + \frac{9}{4\Delta x}\bar{u}_{i+1} - \frac{15}{2\Delta x}\bar{v}_i - \frac{15}{2\Delta x}\bar{v}_{i+1}.
\end{aligned}
$$

By $p_0'(x_{i+\frac{1}{2}}) = \sum_{n=1}^{3}\gamma_n' p_n'(x_{i+\frac{1}{2}})$, we obtain linear weights $\gamma_1' = \frac{11}{459}$, $\gamma_2' = \frac{44}{765}$, $\gamma_3' = \frac{124}{135}$, and define the smoothness indicators for the reconstruction of derivatives as

$$
\beta_n' = \sum_{\alpha=2}^{3}\int_{I_i} \Delta x^{2\alpha-1}\left(\frac{\partial^\alpha p_n(x)}{\partial x^\alpha}\right)^2 dx, \quad n = 1,2,3, \tag{A.1}
$$

then

$$
\begin{cases}
\beta_1' = \dfrac{1}{4}\left(15\bar{u}_{i-1} - 15\bar{u}_i + 66\bar{v}_{i-1} + 114\bar{v}_i\right)^2 + \dfrac{975}{4}\left(\bar{u}_{i-1} - \bar{u}_i + 6\bar{v}_{i-1} + 6\bar{v}_i\right)^2,\\
\beta_2' = \left(\bar{u}_{i-1} - 2\bar{u}_i + \bar{u}_{i+1}\right)^2 + \dfrac{975}{121}\left(\bar{u}_{i-1} - \bar{u}_{i+1} + 24\bar{v}_i\right)^2,\\
\beta_3' = \dfrac{1}{4}\left(15\bar{u}_i - 15\bar{u}_{i+1} + 66\bar{v}_{i+1}\right)^2 + \dfrac{975}{4}\left(\bar{u}_i - \bar{u}_{i+1} + 6\bar{v}_i + 6\bar{v}_{i+1}\right)^2.
\end{cases}
$$

The nonlinear weights are computed as $\omega_n' = \frac{\bar{\omega}_n}{\bar{\omega}_1+\bar{\omega}_2+\bar{\omega}_3}$ with $\bar{\omega}_n = \frac{\gamma_n'}{(\varepsilon+\beta_n')^2}$, $n = 1,2,3$. The final HWENO reconstruction of $(u_x)^-_{i+\frac{1}{2}}$ is given by $(u_x)^-_{i+\frac{1}{2}} = \sum_{n=1}^{3}\omega_n' p_n'(x_{i+\frac{1}{2}})$. Similarly, we can obtain the HWENO reconstruction of $(u_x)^+_{i-\frac{1}{2}}$.

StepA.2. The linear reconstruction of $(u_x)^{\mp}_{i\pm\frac{1}{2}}$.

If no cells in S_0 are identified as troubled cells, then we simply use upwind linear reconstruction for $(u_x)^{\mp}_{i\pm\frac{1}{2}}$:

$$
\begin{aligned}
(u_x)^+_{i-\frac{1}{2}} &= p_0'\left(x_{i-\frac{1}{2}}\right) = -\frac{19\overline{u}_{i-1}}{9\Delta x} + \frac{9\overline{u}_i}{4\Delta x} - \frac{5\overline{u}_{i+1}}{36\Delta x} - \frac{62\overline{v}_{i-1}}{9\Delta x} - \frac{97\overline{v}_i}{18\Delta x} + \frac{11\overline{v}_{i+1}}{18\Delta x},\\
(u_x)^+_{i+\frac{1}{2}} &= p_0'\left(x_{i+\frac{1}{2}}\right) = \frac{5\overline{u}_{i-1}}{36\Delta x} - \frac{9\overline{u}_i}{4\Delta x} + \frac{19\overline{u}_{i+1}}{9\Delta x} + \frac{11\overline{v}_{i-1}}{18\Delta x} - \frac{97\overline{v}_i}{18\Delta x} + \frac{62\overline{v}_{i+1}}{9\Delta x}.
\end{aligned}
$$

StepA.3. The linear reconstruction of $(u_x)_{i\pm\sqrt{5}/10}$.

$$
\begin{aligned}
(u_x)_{i-\frac{\sqrt{5}}{10}} =& p_0'\left(x_{i-\frac{\sqrt{5}}{10}}\right) = -\left(\frac{99\sqrt{5}}{360\Delta x} + \frac{1}{72}\right)\bar{u}_{i-1} + \frac{11\sqrt{5}}{20\Delta x}\bar{u}_i - \left(\frac{99\sqrt{5}}{360} - \frac{1}{72}\right)\bar{u}_{i+1}\\
&- \left(\frac{21\sqrt{5}}{20\Delta x} + \frac{11}{180\Delta x}\right)\bar{v}_{i-1} + \frac{1069\sqrt{5}}{90\Delta x}\bar{v}_i - \left(-\frac{21\sqrt{5}}{20\Delta x} + \frac{11}{180\Delta x}\right)\bar{v}_{i+1},\\
(u_x)_{i+\frac{\sqrt{5}}{10}} =& p_0'\left(x_{i+\frac{\sqrt{5}}{10}}\right) = \left(\frac{99\sqrt{5}}{360\Delta x} - \frac{1}{72}\right)\bar{u}_{i-1} - \frac{11\sqrt{5}}{20\Delta x}\bar{u}_i + \left(\frac{99\sqrt{5}}{360} + \frac{1}{72}\right)\bar{u}_{i+1}\\
&+ \left(\frac{21\sqrt{5}}{20\Delta x} - \frac{11}{180\Delta x}\right)\bar{v}_{i-1} + \frac{1069\sqrt{5}}{90\Delta x}\bar{v}_i + \left(-\frac{21\sqrt{5}}{20\Delta x} - \frac{11}{180\Delta x}\right)\bar{v}_{i+1}.
\end{aligned}
$$

A.2. Two-dimensional case

Similar to the one-dimensional case, firstly, we first identify the troubled cells and modify the first order moment in the troubled cells, see in [32] for detail. Then, we use the HWENO reconstruction in StepA.4 to reconstruct $u_x(G_\ell)$ and $u_y(G_\ell)$ only when G_ℓ is in the interior of a troubled cell $I_{i,j}$. For all other cases, we use the linear reconstruction in StepA.5.

StepA.4. Suppose we have constructed the eight Hermite cubic polynomials $p_1(x,y),\ldots,p_8(x,y)$ in the small stencil and have the explicit expression of these polynomials in [32]. Then we can get the values of the partial derivative of these polynomial at the specific points. To combine the polynomials to obtain third-order approximation to u_x and u_y at the point G_k, we choose the linear weights denoted by $\gamma_{x1}^{(k)},\ldots,\gamma_{x8}^{(k)},\gamma_{y1}^{(k)},\ldots,\gamma_{y8}^{(k)}$ such that

$$
\frac{\partial}{\partial x}u\left(G_k\right) = \sum_{n=1}^{8}\gamma_{xn}^{(k)}\frac{\partial}{\partial x}p_n\left(G_k\right), \quad \frac{\partial}{\partial y}u\left(G_k\right) = \sum_{n=1}^{8}\gamma_{yn}^{(k)}\frac{\partial}{\partial y}p_n\left(G_k\right) \tag{A.2}
$$

which are valid for any quadratic polynomial u. Then we can obtain third-order approximations to u_x and u_y at the point G_k for all sufficiently smooth functions u. Notice that $p_n(x, y)$ is an incomplete Hermite cubic reconstruction polynomial, (A.2) holds for any polynomial u which is a linear combination of 1, x, y, x^2, xy, y^2, x^3, y^3 if $\sum_{n=1}^{8} \gamma_{xn}^{(k)} = 1$ and if $\sum_{n=1}^{8} \gamma_{yn}^{(k)} = 1$ respectively. There are two other constraints on each of the groups of linear weights $\gamma_{x1}^{(k)}, ..., \gamma_{x8}^{(k)}$ and $\gamma_{y1}^{(k)}, ..., \gamma_{y8}^{(k)}$ for (A.2) to hold for $u = x^2 y$, xy^2 respectively. This leaves 5 free parameters in determining each group of the linear weights, obtained uniquely by the least square methodology on $\sum_{n=1}^{8} (\gamma_{xn}^{(k)})^2$ and $\sum_{n=1}^{8} (\gamma_{yn}^{(k)})^2$ respectively.

Similar to the one dimensional case, if G_ℓ is in the interior of a cell $I_{i,j}$ we use linear reconstruction to get $u_x(G_\ell)$ and $u_y(G_\ell)$. Only when G_ℓ is located on the cell boundary of a troubled cell $I_{i,j}$, we use HWENO reconstruction procedures as follows. We compute the smoothness indicator, denoted by β_n:

$$\beta_n = \sum_{|\ell|=2}^{3} \left|I_{ij}\right|^{|\ell|-1} \int_{I_{ij}} \left(\frac{\partial^{|\ell|}}{\partial x^{l_1} \partial y^{l_2}} p_n(x, y) \right)^2 dxdy, \quad n = 1, \ldots 8, \tag{A.3}$$

where $\ell = (\ell_1, \ell_2)$, $|\ell| = \ell_1 + \ell_2$. Computing the nonlinear weights:

$$\omega_{xn}^{(\ell)} = \frac{\overline{\omega}_{xn}^{(\ell)}}{\sum_k \overline{\omega}_{xk}^{(\ell)}}, \overline{\omega}_{xk}^{(\ell)} = \frac{\gamma_{xk}^{(\ell)}}{(\varepsilon+\beta_{xk})^2}, \ \omega_{yn}^{(\ell)} = \frac{\overline{\omega}_{xn}^{(\ell)}}{\sum_k \overline{\omega}_{xk}^{(\ell)}}, \overline{\omega}_{xk}^{(\ell)} = \frac{\gamma_{xk}^{(\ell)}}{(\varepsilon+\beta_{xk})^2}, \ k, \ell = 1, \cdots, 8. \tag{A.4}$$

The HWENO reconstruction to $u_x^-(G_k)$ and $u_y^-(G_k)$ given by $u_x^-(G_\ell) = \sum_{n=1}^{8} \omega_{xn}^{(\ell)} \frac{\partial}{\partial x} p_n(G_\ell)$ and $u_y^-(G_\ell) = \sum_{n=1}^{8} \omega_{yn}^{(\ell)} \frac{\partial}{\partial y} p_n(G_\ell)$. The reconstructions to $u_x^+(G_\ell)$ and $u_y^+(G_\ell)$ are similar.

StepA.5. The linear approximation of the partial derivatives at point G_ℓ can be taken directly by (A.2).

References

[1] X. Cai, J. Qiu, J.-M. Qiu, A conservative semi-Lagrangian HWENO method for the Vlasov equation, J. Comput. Phys. 323 (2016) 95–114.
[2] X. Cai, X. Zhang, J. Qiu, Positivity-preserving high order finite volume HWENO schemes for compressible Euler equations, J. Sci. Comput. 68 (2016) 464–483.
[3] X. Cai, J. Zhu, J. Qiu, Hermite WENO schemes with strong stability preserving multi-step temporal discretization methods for conservation laws, J. Comput. Math. 35 (2017) 52–73.
[4] Z. Chen, H. Huang, J. Yan, Third order maximum-principle-satisfying direct discontinuous Galerkin methods for time dependent convection diffusion equations on unstructured triangular meshes, J. Comput. Phys. 308 (2016) 198–217.
[5] J. Du, Y. Yang, Maximum-principle-preserving third-order local discontinuous Galerkin method for convection-diffusion equations on overlapping meshes, J. Comput. Phys. 377 (2019) 117–141.
[6] R.P. Fedkiw, T. Aslam, B. Merriman, S. Osher, A non-oscillatory Eulerian approach to interfaces in multimaterial flows (the ghost fluid method), J. Comput. Phys. 152 (1999) 457–492.
[7] Y. Guo, T. Xiong, Y. Shi, A positivity-preserving high order finite volume compact-WENO scheme for compressible Euler equations, J. Comput. Phys. 274 (2014) 505–523.
[8] X.Y. Hu, N. Adams, C.-W. Shu, Positivity-preserving method for high-order conservative schemes solving compressible Euler equations, J. Comput. Phys. 242 (2013) 169–180.
[9] V.P. Korobeinikov, Problems of Point Blast Theory, American Institute of Physics, College Park, 1991.
[10] H. Li, S. Xie, X. Zhang, A high order accurate bound-preserving compact finite difference scheme for scalar convection diffusion equations, SIAM J. Numer. Anal. 56 (2018) 3308–3345.
[11] H. Liu, J. Qiu, Finite difference Hermite WENO schemes for hyperbolic conservation laws, J. Sci. Comput. 63 (2015) 548–572.
[12] H. Liu, J. Qiu, Finite difference Hermite WENO schemes for conservation laws, II: an alternative approach, J. Sci. Comput. 66 (2016) 598–624.
[13] X.-D. Liu, S. Osher, T. Chan, Weighted essentially non-oscillatory schemes, J. Comput. Phys. 115 (1994) 200–212.
[14] D. Luo, W. Huang, J. Qiu, A hybrid LDG-HWENO scheme for KdV-type equations, J. Comput. Phys. 313 (2016) 754–774.
[15] H. Luo, J.D. Baum, R. Lohner, A Hermite WENO-based limiter for discontinuous Galerkin method on unstructured grids, J. Comput. Phys. 225 (2007) 686–713.
[16] H. Luo, Y.D. Xia, S.J. Li, R. Nourgaliev, C.P. Cai, A Hermite WENO reconstruction-based discontinuous Galerkin method for the Euler equations on tetrahedral grids, J. Comput. Phys. 231 (2012) 5489–5503.
[17] M.R. Norman, Hermite WENO limiting for multi-moment finite-volume methods using the ADER-DT time discretization for 1-d systems of conservation laws, J. Comput. Phys. 282 (2015) 381–396.
[18] J. Qiu, C.-W. Shu, Hermite WENO schemes and their application as limiters for Runge-Kutta discontinuous Galerkin method: one-dimensional case, J. Comput. Phys. 193 (2004) 115–135.
[19] J. Qiu, C.-W. Shu, Hermite WENO schemes and their application as limiters for Runge-Kutta discontinuous Galerkin method II: two dimensional case, Comput. Fluids 34 (2005) 642–663.
[20] J. Qiu, C.-W. Shu, Hermite WENO schemes for Hamilton-Jacobi equations, J. Comput. Phys. 204 (2005) 82–99.
[21] L.I. Sedov, Similarity and Dimensional Methods in Mechanics, Academic Press, New York, 1959.
[22] Z. Tao, F. Li, J. Qiu, High-order central Hermite WENO schemes on staggered meshes for hyperbolic conservation laws, J. Comput. Phys. 281 (2015) 148–176.
[23] Z. Tao, F. Li, J. Qiu, High-order central Hermite WENO schemes: dimension-by-dimension moment-based reconstructions, J. Comput. Phys. 318 (2016) 222–251.
[24] Z. Tao, J. Qiu, Dimension-by-dimension moment-based central Hermite WENO schemes for directly solving Hamilton-Jacobi equations, Adv. Comput. Math. 43 (2017) 1023–1058.
[25] T. Xiong, J.-M. Qiu, Z. Xu, Parametrized positivity preserving flux limiters for the high order finite difference WENO scheme solving compressible Euler equations, J. Sci. Comput. 67 (2015) 1066–1088.

[26] X. Zhang, On positivity-preserving high order discontinuous Galerkin schemes for compressible Navier-Stokes equations, J. Comput. Phys. 328 (2017) 301–343.
[27] X. Zhang, Y. Liu, C.-W. Shu, Maximum-principle-satisfying high order finite volume weighted essentially nonoscillatory schemes for convection-diffusion equations, SIAM J. Sci. Comput. 34 (2012) A627–A658.
[28] X. Zhang, C.-W. Shu, On positivity-preserving high order discontinuous Galerkin schemes for compressible Euler equations on rectangular meshes, J. Comput. Phys. 229 (2010) 8918–8934.
[29] X. Zhang, C.-W. Shu, Maximum-principle-satisfying and positivity-preserving high-order schemes for conservation laws: survey and new developments, Proc. R. Soc. A, Math. Phys. Eng. Sci. 467 (2011) 2752–2776.
[30] X. Zhang, C.-W. Shu, Positivity-preserving high order finite difference WENO schemes for compressible Euler equations, J. Comput. Phys. 231 (2012) 2245–2258.
[31] Y. Zhang, X. Zhang, C.-W. Shu, Maximum-principle-satisfying second order discontinuous Galerkin schemes for convection-diffusion equations on triangular meshes, J. Comput. Phys. 234 (2013) 295–317.
[32] Z. Zhao, Y.B. Chen, J. Qiu, A hybrid Hermite WENO scheme for hyperbolic conservation laws, J. Comput. Phys. 405 (2020).
[33] Z. Zhao, J. Qiu, A Hermite WENO scheme with artificial linear weights for hyperbolic conservation laws, J. Comput. Phys. 417 (2020).
[34] F. Zheng, J. Qiu, Directly solving the Hamilton-Jacobi equations by Hermite WENO schemes, J. Comput. Phys. 307 (2016) 423–445.
[35] F. Zheng, C.-W. Shu, J. Qiu, Finite difference Hermite WENO schemes for the Hamilton-Jacobi equations, J. Comput. Phys. 337 (2017) 27–41.
[36] F. Zheng, C.-W. Shu, J. Qiu, High order finite difference Hermite WENO schemes for the Hamilton-Jacobi equations on unstructured meshes, Comput. Fluids 183 (2019) 53–65.
[37] J. Zhu, J. Qiu, A class of the fourth order finite volume Hermite weighted essentially non-oscillatory schemes, Sci. China Ser. A, Math. 51 (2008) 1549–1560.
[38] J. Zhu, J. Qiu, Hermite WENO schemes and their application as limiters for Runge-Kutta discontinuous Galerkin method, III: unstructured meshes, J. Sci. Comput. 39 (2009) 293–321.
[39] J. Zhu, J. Qiu, Hermite WENO schemes for Hamilton-Jacobi equations on unstructured meshes, J. Comput. Phys. 254 (2013) 76–92.
[40] J. Zhu, J. Qiu, Finite volume Hermite WENO schemes for solving the Hamilton-Jacobi equation, Commun. Comput. Phys. 15 (2014) 959–980.
[41] J. Zhu, J. Qiu, Finite volume Hermite WENO schemes for solving the Hamilton-Jacobi equations II: unstructured meshes, Comput. Math. Appl. 68 (2014) 1137–1150.
[42] J. Zhu, X.H. Zhong, C.-W. Shu, J. Qiu, Runge-Kutta discontinuous Galerkin method with a simple and compact Hermite WENO limiter, Commun. Comput. Phys. 19 (2016) 944–969.